HHS Public Access

Author manuscript

J Mol Cell Cardiol. Author manuscript; available in PMC 2016 April 01.

Published in final edited form as:

J Mol Cell Cardiol. 2015 April ; 81: 162–175. doi:10.1016/j.yjmcc.2015.02.014.

β-adrenergic effects on cardiac myofilaments and contraction in an integrated rabbit ventricular myocyte model

Jorge A. Negroni[*], **Stefano Morotti**[δ], **Elena C. Lascano**[*], **Aldrin V. Gomes**[↓], **Eleonora Grandi**[δ], **José L Puglisi**[δ], and **Donald M. Bers**[δ]

[*]Department of Comparative, Cellular and Molecular Biology, Universidad Favaloro, Buenos Aires, Argentina

[↓]Department of Neurobiology, Physiology and Behavior, University of California Davis, CA

[δ]Department of Pharmacology, University of California Davis, CA

Abstract

A five-state model of myofilament contraction was integrated into a well-established rabbit ventricular myocyte model of ion channels, Ca^{2+} transporters and kinase signaling to analyze the relative contribution of different phosphorylation targets to the overall mechanical response driven by β-adrenergic stimulation (β-AS). β-AS effect on sarcoplasmic reticulum Ca^{2+} handling, Ca^{2+}, K^+ and Cl^- currents, and Na^+/K^+-ATPase properties were included based on experimental data. The inotropic effect on the myofilaments was represented as reduced myofilament Ca^{2+} sensitivity (XBCa) and titin stiffness, and increased cross-bridge (XB) cycling rate (XBcy). Assuming independent roles of XBCa and XBcy, the model reproduced experimental β-AS responses on action potentials and Ca^{2+} transient amplitude and kinetics. It also replicated the behavior of force-Ca^{2+}, release-restretch, length-step, stiffness-frequency and force-velocity relationships, and increased force and shortening in isometric and isotonic twitch contractions. The β-AS effect was then switched off from individual targets to analyze their relative impact on contractility. Preventing β-AS effects on L-type Ca^{2+} channels or phospholamban limited Ca^{2+} transients and contractile responses in parallel, while blocking phospholemman and K^+ channel (I_{Ks}) effects enhanced Ca^{2+} and inotropy. Removal of β-AS effects from XBCa enhanced contractile force while decreasing peak Ca^{2+} (due to greater Ca^{2+} buffering), but had less effect on shortening. Conversely, preventing β-AS effects on XBcy preserved Ca^{2+} transient effects, but blunted inotropy (both isometric force and especially shortening). Removal of titin effects had little impact on contraction. Finally, exclusion of β-AS from XBCa and XBcy while preserving effects on other targets resulted in preserved peak isometric force response (with slower kinetics) but nearly

Correspondence: Jorge A. Negroni, Department of Biology, Universidad Favaloro, Solís 453., 1078 Buenos Aires, Argentina, Phone: 5411-4378-1187, Fax: 5411-4381-0323, cardiomod@gmail.com; Donald M. Bers, Department of Pharmacology, University of California Davis, GBSF rm 3513, 451 Health Sciences Drive, Davis, Ca 95616, USA, Phone: 530-752-6517, Fax: 530-752-7710, dmbers@ucdavis.edu.

Disclosures: None declared.

abolished enhanced shortening. β-AS effects on XBCa vs. XBcy have greater impact on isometric vs. isotonic contraction, respectively.

Keywords

β-adrenergic; myocyte model; contractile model; Ca^{2+} sensitivity; cross-bridge cycling

1. Introduction

β-adrenergic stimulation (β-AS) is an important physiological modulator of cardiac activity, increasing peak force (inotropy) and the rate of force development and relaxation (lusitropy). β-AS raises intracellular cAMP levels, activating protein kinase A (PKA), which in turn phosphorylates key proteins involved in excitation-contraction (E–C) coupling. These include the L-type Ca^{2+} channel [1, 2] and phospholamban (PLB), respectively increasing Ca^{2+} entry into the cytoplasm and sarcoplasmic reticulum (SR) Ca^{2+} reuptake by the SR Ca^{2+}-ATPase2a (SERCA2a) [3, 4], and these effects contribute to increased SR Ca^{2+} content, inotropy and lusitropy. High SR Ca^{2+} load also increases Ca^{2+} leak and fractional Ca^{2+} release during E-C coupling [5]. β-AS can increase the probability of ryanodine receptor Ca^{2+} release channel (RyR2) opening in response to cytosolic Ca^{2+} [6], but that may be mediated more by Ca^{2+}/calmodulin-dependent protein kinase II (CaMKII) activation, downstream of nitric oxide synthase (nNOS) or Epac (exchange protein activated by cAMP) [7–11]. K^+ channels are also targets of PKA phosphorylation and can shorten action potential (AP) duration (APD) [12, 13] during β-AS.

At the myofilaments, PKA phosphorylates troponin I (TnI) and myosin binding protein-C (MyBP-C) [14–17]. Although experimental studies have attempted to link specific contractile effects of β-AS to specific TnI and MyBP-C phosphorylation sites, precise roles in altering myofilament Ca^{2+} sensitivity (XBCa) and cross-bridge (XB) cycling rate (XBcy) are still debated. Some studies have suggested that PKA phosphorylation of TnI predominates in both decreased XBCa and enhanced XBcy [18], and the optimization of cardiac function at different heart rate, load and inotropic state [19]. Conversely, it was postulated that TnI and MyBP-C phosphorylation have separate effects on XBCa and XBcy [20, 21], a shared responsibility in PKA-dependent decrease of XBCa [22, 23], or a central role of MyBP-C in the PKA-dependent increased XBcy kinetics [22]. However, the relative PKA effects of these two proteins on twitch contractions, Ca^{2+} transients and APs is lacking. A computational model, as we describe here, can be a valuable complementary tool for further analysis of the impact of XBCa and XBcy and their interaction during β-AS induced inotropy.

Myocyte models have evolved from mathematical descriptions of ion channels to detailed formulations of Ca^{2+} transport mechanisms [24, 25], cell compartmentalization [25, 26], cell signaling pathways [27–30], metabolic processes [31], and pH regulation [32]. Even though mechanical models of the cardiac muscle have been developed [33], they have typically been divorced from electrical/Ca^{2+} handling models [34–37]. Some studies have begun to fill this gap, including descriptions of length and force-dependent processes of Ca^{2+}-induced

XB formation [38] and length-dependent activation [39], but most have been limited to myocyte ion handling and electrophysiological descriptions [27, 29, 40].

The purpose of this study is three-fold: (1) to help clarify unresolved questions of how altered Ca^{2+} sensitivity and XB cycling rate interact during β-AS in ventricular myocytes (and how putative TnI and MyBP-C effects may interact), (2) to provide a new quantitative framework to study the complex interaction of β-AS dynamic effects on Ca^{2+} transient, AP, and contractile properties, which are not well resolved, and (3) to provide a freely available new tool for all investigators to further study these aspects. We have built the β-AS effect on our prior detailed contraction model [37] and incorporated that into an updated Soltis-Saucerman model [29], which integrates the Shannon-Bers Ca^{2+}-electrophysiological myocyte model [25] with dynamic descriptions of CaMKII and PKA signaling pathways [28, 41] and dynamic target phosphorylation.

2. Methods

2.1 Generation of XB force

Our previously described mechanical model [37] has been slightly modified. It represents a muscle or myocyte as a series arrangement of units, each defined by the half-sarcomere length and the muscle cross-sectional area. The half-sarcomere is composed of inextensible thick and thin filaments in parallel with an internal elastic load (Fig. 1A). The thick (ThF) and thin filaments (Tf) can slide past each other defining a zone of overlap where XBs can attach to the thin filament. According to the XB theory, attached XBs act as independent force generators, occupying different states in the XB cycle [42]. Individual XB force is $f_i = a \times h_i$, where **a** is the elastic constant of one attached XB and hi = XB elongation. Then, total XB force (Ft) is:

$$F_t = \sum f_i = a \sum h_i = N \times a \times (\sum h_i / N) \quad (1)$$
$$F_t = N \times a \times h$$

where N is number of attached XBs, N × a represents the elastic constant corresponding to the pool of attached XBs and h is the mean elongation of all XBs. Thus, Ft is the force of an equivalent XB, representing all attached XBs, and h is the equivalent XB length.

Total XB force is normalized for cross-sectional area (Fb) measured at a defined reference state:

$$F_b = F_t / \text{reference area} \quad (2)$$

where reference area = vol_r/L_r with vol_r = half-sarcomere volume of myoplasmic compartment (Bulk Cytosol) containing the mechanical elements and L_r = half-sarcomere slack length, i.e, resting conditions for force close to zero. Then, substituting Eq. 1 into Eq. 2 gives:

$$F_b = N \times a \times h \times L_r / vol_r \quad (3)$$

Since N = Avogadro's number (A) × (moles of attached XBs), it can be expressed as:

$$N = A \times [XB] \times vol_r$$

where [XB] is total attached XB concentration (see Ca^{2+} kinetics). Replacing N in Eq. 3:

$$F_b = A \times [XB] \times a \times h \times L_r$$

Grouping $A \times a \times L_r$ and changes in concentration units into A_e, results in:

$$F_b = A_e \times [XB[\times h \quad (4)$$

The equivalent XB is considered to be situated at the free end of the half myosin filament. Consequently, in the model, half-sarcomere length (L) has two components: an elastic component (h) and a non-elastic component (X) formed by the half-sarcomere thick filament and the parts of the thin filament not overlapping either with the thick filament or h (Fig. 1A). Then:

$$L = X + h \quad (5)$$

We assume that individual XBs attach and detach cyclically and asynchronously from the thin filament, but the equivalent XB remains attached while there is at least one attached XB. In steady state conditions, the equivalent XB has a constant length h_r and during a quick sarcomere shortening equal to ΔL, h instantly absorbs this length change (Fig. 1B), so: $h = h_r - \Delta L$.

The equivalent XB then detaches and reattaches in a different position along the thin filament to return to h_r. This is represented as sliding of the point of attachment of the equivalent XB to reproduce the asynchronous behavior of individual XBs. Thus, the return to h_r produces a change in X expressed as the differential equation:

$$dX/dt = B \times (h - h_r) \quad (6)$$

and substitution by Eq. 5 gives:

$$dX/dt = B \times (L - X - h_r) \quad (7)$$

where dX/dt is the velocity of motion of the mobile equivalent XB end and B is the involved parameter [43]. The sliding movement can also be expressed from the derivation of Eq. 5 and substitution by Eq. 7 as:

$$dL/dt = B \times (h - h_r) + dh/dt. \quad (8)$$

Thus, once shortening ends, dL/dt = 0 and in Eq. 8 returns h exponentially to h_r. Similar criteria apply to the description of muscle stretching and concomitant XB elongation.

Similarly to our previous model [37], two states of attached XBs are defined: XB_w (weak state, with $h = h_w$), a state in which the equivalent XB is attached to the filament but has not

yet developed the power stroke, and XB_p (power state, with $h = h_p$), a state in which the equivalent XB can develop the power stroke [36]. Contrary to XB_p, XB_w elongation h_{wr} is assumed close to zero in steady state conditions. However, when the muscle shortens or stretches, the XB_w elastic element is passively stretched, $h_w \neq 0$, and XB_w respectively contributes negatively or positively to F_b. Then, according to Eq. 4, total XB force becomes:

$$F_b = A_w \times [XB_w] \times h_w + A_p \times [XB_p] \times h_p \quad (9)$$

where A_w and A_p are elastic constants for the weak and power states. According to this assumption Eq. 5 becomes:

$$L = X_w + h_w$$

and

$$L = X_p + h_p$$

showing that for the same L, the inextensible X lengths and the equivalent XB elastic lengths differ according to the XB state. Similarly, from Eq. 8, the two equivalent XB kinetic equations are:

$$dL/dt = B_w \times (h_w - h_{wr}) + dh_w/dt \quad (10)$$

$$dL/dt = B_p \times (h_p - h_{pr}) + dh_p/dt \quad (11)$$

where B_w and B_p are the weak and power parameters.

2.2 Parallel and series elasticity

As shown in Fig. 1A, the muscle unit includes an undamped parallel elastic element that symbolizes the sum of the non-linear titin and the linear cellular passive element components attributed to intermediate filaments (Fig. S1); then, parallel elastic force (F_p) results as:

$$F_p = K_e (L - L_o)^5 + L_e (L - L_o) \quad (12)$$

where K_e and L_e, respectively represent titin and cellular element elasticities for F_p normalized by cross-sectional area, and L_o is slack length (L for $F_p = 0$). Then, total muscle force (F_m) is the sum of F_b plus the force needed to stretch F_p:

$$F_m = F_b + F_p.$$

An elastic element in series with the muscle (Fig. 1A) is added to describe compliant muscle ends, producing elastic force F_s:

$$F_s=F_m=\alpha\times(e^{\beta L_S}-1) \quad (13)$$

where α and β are parameters defining the elastic relation and L_s is series elastic length, showing that changes in F_m produced by F_b elicit changes in L_s. Then, total muscle length (L_m) results as:

$$L_m=L_s+L.$$

Therefore, according to the model, in isometric conditions, changes in F_m produced by F_b generation trigger changes in L_s and hence in L because L_m is constant. Variations in L then lead to h changes whose return to h_r is achieved through Eq. 6. In isotonic conditions, where F_m is constant, F_b and F_p change due to L variations, and again these L changes lead to h adjustments with the ensuing return to h_r through Eq. 6. Finally, in isosarcometric contractions L is constant, $L_s = 0$, and consequently $L_m = L$ [37].

2.3 Myofilament Ca^{2+} kinetics

Ca^{2+} kinetics is represented by five states of troponin systems (TS) (Fig. 1C), which is a slight simplification of the prior six state model [37], by condensing an intermediate state (TS˜) into the TS* to TS transition. Each TS is defined as 3 adjacent troponin-tropomyosin regulatory units (RU) [36], so that each can bind one Ca^{2+} ion (TSCa, $TSCa_2$, $TSCa_3$). In this scheme, Ca^{2+} binding to the three RU within one TS is cooperative, and we assume that all three Ca^{2+} bind in one step (so only $TSCa_3$ is indicated) driven by the on- and off-rate constants (Y_b and Z_b, Fig. 1C), where $[Ca^{2+}]i$ is free Ca^{2+} concentration in the bulk cytosol. It is further postulated that XB attachment takes place when Ca^{2+} RUs are fully activated and driven by the forward (f) and reverse (g) rate constants. The five TS states are thus: TS (free); $TSCa_3$ (Ca^{2+} bound to TS, without XB attachment), $TSCa_3$~ (weak binding XB (XB_w) with Ca^{2+} bound to TS), and TS* (attached XBs in the power state (XB_p) involving TS without Ca^{2+}). Because force depends on attached [XB], Eq. 9 results as:

$$F_b=A_w(3[TSCa_3{}^{\sim}])h_w+A_p(3[TSCa_3*])+3[TS*]h_p \quad (14)$$

and redefining A_p and A_w to include the common factor 3 gives:

$$F_b=A_w([TSCa_3{}^{\sim}])h_w+A_p([TSCa_3*])+[TS*]h_p. \quad (15)$$

Rates of change of TS states (Fig 1C) are described by the following differential equations:

$$d[TSCa_3]/dt=Y_b[TS][Ca^{2+}]i^3-Z_b[TSCa_3]+g[TSCa_3{}^{\sim}]-f[TSCa_3] \quad (16)$$

$$d[TSCa_3{}^{\sim}]/dt=f[TSCa_3]-g[TSCa_3{}^{\sim}]+Z_p[TSCa_3*]-Y_p[TSCa_3{}^{\sim}] \quad (17)$$

$$d[TSCa_3*]/dt=Y_p[TSCa_3{}^{\sim}]-Z_p[TSCa_3*]+Z_r[TS*][Ca^{2+}]i^3-Y_r[TSCa_3*] \quad (18)$$

$$d[TS*]/dt = Y_r[TSCa_3*] - Z_r[TS*][Ca^{2+}]i^3 - gd[TS*] \quad (19)$$

and introducing [TSt] as total concentration, the five TS can be expressed as:

$$[TS] = [TSt] - [TSCa_3] - [TSCa_3\tilde{}] - [TSCa_3*] - [TS*[, \quad (20)$$

where Y_b, Z_b, f, g, Y_p, Z_p, Y_r, Z_r, and g_d are reaction rate parameters with subscripts b, p, r and d respectively related to **b**inding of Ca^{2+}, **p**ower state transition, **r**eversal of Ca^{2+} binding and **d**issociation of XB (Fig 1C).

The model utilizes three length-dependent reaction rate parameters. The first is the sarcomere attachment rate function which accounts for XB attachment in the zone of overlap between thick and thin filaments [42]:

$$f = Y_a \times e^{-R_a(L-L_a)^2} \quad (21)$$

where L_a is the optimal overlap length for maximum XB attachment, Y_a is maximum f for L = L_a and R_a commands the kurtosis of the curve, changing the effective zone of overlap between thin and thick filaments [37, 43]. The second is the redefined velocity-dependent XB detachment rate constant g, with the asymmetrical detachment behavior postulated by Huxley [42] (Fig. 2A):

$$g = Z_a + Y_h \quad (22)$$

where Y_h is the detachment function characterized as

$$Y_h = F_h \times Y_v \times (1 - e^{-\gamma(h_w - h_{wr})^2}). \quad (23)$$

In Eq. 23, $(1 - e^{-\gamma(hw - hwr)})$ represents the symmetrical detachment function used by Slawnych *et al.* [44] where γ defines the kurtosis of the curve and sarcomere L velocity dependence through (h_w-h_{wr}), F_h provides asymmetry [42] (with F_h = 0.1 or F_h = 1 for $h_w > h_{wr}$ or $h_w < h_{wr}$, respectively), Y_v amplifies the detachment effect, and Z_a is a constant representing the value of g when $h_w = h_{wr}$. This more accurate g description resulted in improved simulation of afterloaded contractions (Fig. 2B). The third is the sarcomere length-dependent rate function of XB detachment from TS* to TS given by:

$$g_d = Y_d \times e^{-Y_C(L-L_C)} \quad (24)$$

where L_c determines the range of sarcomere length around which g_d varies, Y_c defines the rate of change of g_d, and Y_d is the value of g_d for L = L_c. This equation represents the lattice space effect on the rate of XB detachment whereby g_d decreases at larger lengths reducing lattice space [45].

To express Ca^{2+} binding and buffering by myofilaments, the low affinity troponin C (TnC_{low}) Ca^{2+} buffer in the Soltis-Saucerman model [29] (from the Shannon-Bers model [25]) was interpreted as the sum of change of all TS bound to Ca^{2+}:

$$d[TnC_{low} \cdot Ca]/dt = 3(d[TSCa_3]/dt + d[TSCa_3^{\sim}]/dt + d[TSCa_{3*}]/dt) \quad (25)$$

expressing buffer action dependence on the contractile machinery and hence on L_m and F_m and the mode of contraction.

Table 1 shows the classification of contractile parameters. One group of parameters is structural (Strct). A second group of parameters corresponds to XBCa, involving the rate constants Y_b, Z_b, Y_r and Z_r acting in transitions where there are only changes in Ca^{2+} binding to TS with no modifications in the XB force generating capacity. The third group of parameters comprises XBcy rate constants Z_p and Y_p, and parameters related to rate functions g, f, and g_d, acting in transitions of XB attachment and detachment, altering the force generating capacity and cycling rate without producing changes in Ca^{2+} binding to TS.

2.4 Integrated ionic, contractile, and β-AS model

We embedded the contraction model with the Soltis-Saucerman model [29], and updated the formulation of target phosphorylation by PKA in several ways (detailed in the Supplement): (1) I_{Ks} phosphorylation kinetics were slowed, as done previously [46] in accordance with recent experimental observations [47]; (2) phosphorylation of phospholemman (PLM) to increase Na^+–K^+-ATPase (NKA) affinity for internal Na^+ [48] was added as done previously [30, 46, 49, 50]; (3) PKA-dependent modulation of I_{Kr} was introduced based on experiments by Harmati *et al.* [51] with kinetics that we used for I_{Ks} phosphorylation previously [52]; (4) formulation of PKA-dependent modulation of $I_{Cl(}Ca)$ [53] was added with the same kinetics as for CFTR phosphorylation. Figure S2 shows the responses of ionic PKA targets to isoproterenol (ISO), and Table 2 describes the effects of 100 nM [ISO] administration; (5) PKA-dependent effects on contraction were added, with phosphorylation extent and kinetics as was formulated for TnI in the Soltis-Saucerman model. Table 1 reports all changes to myofilament model parameters induced by 100 nM [ISO] administration. PKA phosphorylation has been reported to reduce stiffness (attributed to titin) [54] and XBCa [55], in addition to increasing XBcy [18, 20–22]. The maximal ISO-induced reduction of titin stiffness was represented by decreasing the parallel element elasticity (K_e) by 50% to explain sarcomere passive force reduction with β-AS [56] (see Supplement and Fig. S3). To reproduce PKA effects on contractile targets, XBCa was adjusted by increasing the rate constants Zb, Yr and Zr to reduce Ca^{2+} affinity and alter the ratio of Ca^{2+} binding over unbinding rate parameters (Yb/Zb and Yr/Zr) favoring Ca^{2+} release. The ISO effect on XBcy was represented by modifying the rate constants Zp, Yp and parameters involved in g, f, and g_d to increase the rate constants implicated in XB attachment and detachment (Fig. 1C).

All simulations were performed in MATLAB (The MathWorks, Natick, MA, USA) using the stiff ordinary differential equation solver ode15s. The model code is available for download at: https://somapp.ucdmc.ucdavis.edu/Pharmacology/bers/.

3. Results

3.1 β-AS behavior at imposed $[Ca^{2+}]$

Figures 3 and 4 and Table 3 show results of control and β-AS at fixed $[Ca^{2+}]_i$, to assess PKA effects on XBCa and XBcy separately, independent of $[Ca^{2+}]_i$ changes. We compared simulations to experiments done in transgenic animals in which PKA phosphorylation on TnI or MyBP-C sites was prevented. To this end, abrogation of the ISO-induced XBCa desensitization was simulated by eliminating ISO effects on parameters involved in XBCa (ISO-XBCa), and to suppress ISO-increased XBcy we removed ISO effects on XBcy parameters (ISO-XBcy). Simulations were compared with skinned fiber data in the literature. Fig. 3A illustrates experimental (top) [20] and model (bottom) for XB force (F_b) vs. $[Ca^{2+}]_i$ relationships at halfsarcomere length of 1.05 μm. Skinned fibers often exhibit higher half-activating $[Ca^{2+}]_i$ ($[Ca^{2+}]_{50}$) vs. measurements in intact fibers or myocytes, due partly to supra-physiological free $[Mg^{2+}]$ in the former [57], which would prevent contraction for normal myocyte Ca^{2+} transients (below 1 μM). Our control half-activating $[Ca^{2+}]_{50}$ = 0.79 μM and apparent Hill coefficient (3.6) agrees with baseline data in intact muscle. From this baseline, ISO produced a rightward shift of the force-$[Ca^{2+}]$ relationship, as seen experimentally. ISO-XBcy behavior was comparable to that of ISO, as reported in transgenic mice expressing non-phosphorylatable MyBP-C [20]. ISO-XBCa reversed the ISO relationship towards control as observed by Kentish *et al.* in mice expressing non phosphorylatable TnI [18]. In simulation-generated values fitted to the Hill equation [37, 58], ISO caused a rightward shift of 51% in $[Ca^{2+}]_{50}$ with only slight changes in Hill coefficient (nH) and F_b(max), in agreement with experimental studies in mouse skinned cardiac muscle [18, 20], ferret papillary muscle [59] and rat trabeculae [60].

Figure 3B (top) shows an experimental stiffness-frequency relationship [18] reflecting actively cycling XB kinetics and Fig. 3B (bottom) depicts simulation results. Simulation of experimental stiffness-frequency relationships [61] has been previously described [37, 43]. These were obtained at steady-state with sinusoidal oscillations from a constant basal L (Lbas) to give an input L(t) = Lbas + ΔL sin(2π freq t), where ΔL (< 1% of Lbas) is the amplitude and freq the frequency of the applied oscillations. The stiffness modulus is defined as ΔF/ΔL, where ΔF is the amplitude of the resulting force oscillations. Stiffness simulations showed a minimum at 0.85 Hz frequency in control conditions. ISO produced a 41% rightward shift of this relationship, within the range experimentally reported (19% [62] and 63% [18]). ISO-XBCa only slightly limited the ISO effect (32% vs. 41% rightward shift vs. control), a change that was less pronounced than that seen in non-phosphorylatable TnI mice [18]. Conversely, ISO-XBcy completely abrogated the shift in stiffness minimum, suggesting that XBcy is more important than XBCa in the dynamic stiffness response to ISO.

Figure 3C shows the effect of β-AS on XB kinetics assessed by force-velocity relationships. Similarly to experimental results (top panel) [63], simulated isotonic shortening velocities during force clamps at constant $[Ca^{2+}]_i$ (2 μM) (bottom panel) showed that ISO enhanced shortening velocity at every force value. Maximal velocity at F_m = 0 increased by 60%, comparable to experiments in cat papillary muscle with norepinephrine [64] and rat

myocytes with PKA stimulation [63]. ISO-XBCa produced a similar result (65% increase with respect to control) while ISO-XBcy abolished the ISO-induced response, suggesting that, like the dynamic stiffness behavior, XBcy predominates on the force-velocity reaction in enhanced inotropic state.

Figure 4A (top, left) shows experimental muscle force (F_m) response to 1% step increase in muscle length (L_m) [21]. Following the length step the apparent rate constant of force decay (k_{rel}) indicates rates of detachment/reattachment of strongly bound XBs, and the apparent rate constant of force redevelopment (k_{df}) indicates XB recruitment into the force-generating state. Simulation results (Fig. 4A, right) show F_m responses to a similar 1% stretch. The insets illustrate more clearly that ISO increased k_{rel} by 157% and k_{df} by 124% (Table 3). As expected, a similar response was observed for ISO-XBCa, comparable to reported effects in wild type and non-PKA phosphorylatable TnI transgenic mice [21]. On the other hand, ISO-XBcy reversed the response towards control, suggesting major XBcy involvement in the k_{rel} response, in accordance with the behavior observed in mice with non-phosphorylatable MyBP-C sites [20].

XB kinetics were also assessed during release-re-stretch (20%) from half-sarcomere length = 1.05 μm, lasting 20 ms at $[Ca^{2+}]_i$ = 0.75 μM, as done experimentally [23, 65] (Fig. 4B, bottom right). The rate of force redevelopment (k_{tr}) following the length pulse (determined at half-time force recovery [66], upper panel) was 2.98 s^{-1} in control, similar to the linear slope of two phase k_{tr}-pCa Hill plots (3.21–1.83 s^{-1}) reported in similar conditions in isolated rat myocytes [65]. ISO increased k_{tr} by 46% and further enhanced it by 68% in ISO-XBCa, comparable to experiments on PKA-treated wild type and non-phosphorylatable TnI rat ventricular trabeculae Fig 4B, right) [23]. Preventing the cycling rate effect (ISO-XBcy) abolished the ISO-induced increase in k_{tr}, which was decreased even below control. Taken together, these results suggest that both XBCa and XBcy influence k_{tr}.

3.2 β-AS effect on action potentials, Ca^{2+} transients and contractions

Figures 5 and 6 and Tables 4 and S1 show effects of β-AS on 1 Hz steady state AP, Ca^{2+} transients and contractions for intact myocyte twitches. We separately assessed the impact of each PKA target. ISO (100 nM) decreased APD only slightly (from 211 to 204 ms), consistent with some experimental data [67, 68]. This is due to a balance of effects on I_{CaL} and PLM which would prolong APD vs. I_{Ks} which would shorten APD. That is, in Fig. 5A, switching off the I_{CaL} effect (blue AP) allows ISO to shorten APD, whereas disabling the I_{Ks} effect allows ISO to prolong APD (Fig 5D). Removing the PLM effect allows $[Na^+]_i$ to rise and increases outward (repolarizing) Na^+-pump current Fig 5C). ISO effects on PLB (Fig. 5B), RyR, I_{Kr}, I_{CFTR} and I_{Cl}(Ca) (Fig. S5) or myofilaments (Fig. 6A) had no appreciable effects on APD.

ISO had the expected effects on Ca^{2+} transients and contraction, increasing the amplitude and rising rate of both and also greatly accelerating $[Ca^{2+}]_i$ decline and relaxation (TCa_{50} and TCa_{90} in Table 4) [59, 62]. The ISO effects on I_{CaL} and PLB were important to the increase in Ca^{2+} transients and contraction amplitude, because preventing either (especially I_{CaL}) reduced peak $[Ca^{2+}]$i and inotropy (Fig. 5A–B). Conversely, the ISO effects on PLM (by limiting $[Na^+]_i$) and I_{Ks} (by limiting APD) both diminish Ca^{2+} loading, Ca^{2+} transient

increases and the inotropic effect seen with ISO (Fig. 5C–D). As expected, PLB effects are important for the ISO-induced acceleration of $[Ca^{2+}]_i$ decline and relaxation. None of the other ion transporters (RyR, I_{Kr}, CFTR, $I_{Cl}(Ca)$) contribute substantially to the effects of ISO on $[Ca^{2+}]_i$ or contraction (Fig. S5).

3.3 β-AS effect on twitch contractions driven by action potentials

Figure 6B shows that the ISO-induced increase in peak $[Ca^{2+}]_i$ and kinetics of the Ca^{2+} transient was unaltered in ISO-XBcy. However, preventing the ISO-induced decrease in myofilament Ca^{2+} affinity (ISO-XBCa and ISO-XBCa-XBcy) reduced peak $[Ca^{2+}]_i$ in response to ISO by 27%, and thus blunted the ISO-induced increase in $[Ca^{2+}]_i$ by 55%. This emphasizes the quantitative impact of myofilament Ca^{2+} buffering during the normal Ca^{2+} transient [69, 70], and that part of the normal ISO-induced increase in Ca^{2+} transients is caused by the reduction in myofilament Ca^{2+} buffering. Thus greater myofilament Ca^{2+} binding in ISO-XBCa (vs. ISO) results in higher force development (Fig. 6C).

Rapid buffering of cytosolic Ca^{2+} is dominated by TnC and SERCA, which are present at 70 and 47 μM respectively [69]. Notably, ISO reduces TnC affinity and increases SERCA affinity for Ca^{2+}. So, with respect to overall cytosolic Ca^{2+} buffering these two effects would tend to partially offset each other, as shown experimentally [70]. Consequently, ISO may have little net effect on cytosolic Ca^{2+} buffering. But with only the SERCA effect (ISO-XBCa) net Ca^{2+} buffering is increased so the same amount of total SR Ca^{2+} release will produce less rise in free $[Ca^{2+}]_i$ (ISO-XBCa vs. ISO in Fig. 6B).

APs were almost identical in ISO vs. ISO-XBCa (APD_{90} = 204 vs. 201 ms; Table 4), despite the much smaller Ca^{2+} transient in ISO-XBCa. Given the importance of Ca^{2+}-dependent currents (e.g. I_{CaL}, Na^+-Ca^{2+} exchanger (NCX) current (I_{NCX}), and $I_{Cl(Ca)}$) the superimposable APs are surprising. The reason is that the change in myofilament Ca^{2+} binding is relatively isolated from the cleft and subsarcolemmal space (Sub-SL, Fig. 1C). During I_{CaL} and SR Ca^{2+} release, the cleft $[Ca^{2+}]$ ($[Ca^{2+}]_{CL}$) is almost uninfluenced by the difference in TnC Ca^{2+} buffering, but rather depends mainly on Ca^{2+} fluxes into the cleft, local buffering in the cleft and diffusion out to the Sub-SL (see Supplement and Fig. S4). Note that the amount and kinetics of Ca^{2+} released in ISO and ISO-XBCa are almost identical. The Sub-SL (where all non-cleft Ca^{2+}-sensitive channels and transporters are) is only somewhat less isolated than the cleft from the myofilaments. That is, during release $[Ca^{2+}]_{CL}$ drives up $[Ca^{2+}]$ in the Sub-SL ($[Ca^{2+}]_{SL}$, which is unaltered by TnC buffering), while diffusion from the Sub-SL to bulk cytosol is only slightly slowed by the higher $[Ca^{2+}]_i$ in ISO vs. ISO-XBCa. Most of the diffusional driving force ($[Ca^{2+}]_{SL} - [Ca^{2+}]_i$) comes from the high $[Ca^{2+}]_{SL}$. The result is that the altered myofilament buffering has no effect on cleft Ca^{2+} channels (I_{CaL} and RyR) and only slight effects on non-cleft Ca^{2+}-dependent currents like I_{NCX}. If we double the diffusion constants for Ca^{2+} and Na^+ from Sub-SL to cytosol, then $[Ca^{2+}]_{SL}$ is still almost unchanged. In contrast, if we reduce SR Ca^{2+} release by 50%, that produces strong and relatively proportional decreases in $[Ca^{2+}]_{CL}$, $[Ca^{2+}]_{SL}$ and $[Ca^{2+}]_i$ (and of course I_{CaL} inactivation, I_{NCX} and APD).

Figure 6C shows isometric twitch force (F_m) at 1 Hz stimulation and L_m = 1.05 μm. ISO increased peak F_m 2.4 fold, and accelerated relaxation, reducing RT_{50} (time from peak to

50% decline) by 29% and T_{90} (time from stimulus to 90% relaxation) by 26%, similar to results obtained in rat trabeculae [71]. As noted above, peak F_m was further enhanced in ISO-XBCa vs. ISO, but the ISO-induced lusitropy was partially reversed, suggesting that ~59% of the lusitropic effect may be due to XBCa effects, while the remaining 41% may be due to PLB-SERCA effects. That is consistent with the 11% acceleration of $[Ca^{2+}]_i$ decline with ISO-XBCa vs. Control, and the slowing of $[Ca^{2+}]_i$ decline and relaxation when PLB phosphorylation is blocked (Fig. 6B). Thus, both myofilament Ca^{2+} desensitization and enhanced SERCA pumping contribute to ISO-induced lusitropy.

Preventing the ISO-induced increase in XB cycling (ISO-XBcy) attenuated the ISO-induced inotropy, despite the normal increase in peak $[Ca^{2+}]_i$. ISO-XBcy also exhibited faster relaxation. This emphasizes not only the critical role of enhanced XB cycling to ISO-induced inotropy, but also that it may slightly limit lusitropy (which seems counter-intuitive). When both cycling and Ca^{2+} binding were suppressed (ISO-XBCa-XBcy) peak force was similar to that with ISO (2.2-fold increase), but contraction duration (both rise and fall) was substantially delayed vs. ISO (TP_{50} was near the control value). The result is that the negative inotropic effect of reduced myofilament Ca^{2+} sensitivity with ISO is compensated by the faster XB cycling, allowing larger and faster isometric contraction, and both factors contribute to faster relaxation with ISO.

Figure 6D shows isotonic contractions (at $F_m = 0.87$ mN.mm^{-2}), where ISO increased maximal shortening (by 88%) and caused faster relaxation, as seen experimentally [72]. Compared to the isometric case, ISO-XBCa only slightly enhanced shortening vs. ISO, and the main effect was a prolongation of contraction time. Thus, the ISO-induced reduction in myofilament Ca^{2+} sensitivity is less limiting for isotonic shortening (at low load) than it is for isometric force. Failure to boost XB cycling (ISO-XBcy) blunted shortening rate and extent vs. ISO (as with F_m), but in this case the combination ISO-XBCa-XBcy was unable to appreciably restore maximum shortening to the ISO level (unlike the isometric case).

Elimination of ISO effects on titin stiffness while preserving it on the other targets (ISO-titin) (Tables 3 and 4) only affected passive force F_m(min) in isometric twitches, with only very slight slowing of force development and decline compared with ISO. In isotonic conditions where force was the imposed variable (and was constant), ISO-titin slowed relengthening by ~7%. These results are consistent with a contribution of titin phosphorylation to restoring force as seen in experimental and simulation restoring force studies [56] (see Supplement and Fig. S6).

Removing the effect of ISO from all myocyte ion fluxes while preserving its effect on myofilaments (ISO-Cytofl) abolished inotropy; in fact, peak force was 12% lower than control. This emphasizes the importance of enhanced Ca^{2+} transients for ISO-induced inotropy. It also shows that the reduced XB Ca^{2+} affinity with ISO slightly supersedes the enhanced XB cycling with respect to isometric force development. Note also that peak $[Ca^{2+}]_i$ is higher than control for ISO-Cytofl, mainly because of the lower Ca^{2+} buffering by myofilaments. For the isotonic case, the ISO-enhanced shortening (88%) was only partially reduced (51%) in ISO-Cytofl. This again emphasizes that enhanced XB cycling is

particularly important for ISO effects on isotonic shortening at low load. Obviously as the load increases the isotonic results would gradually shift to be more like the isometric case.

3.4 Kinetics and dose-dependence of β-AS effect on twitch contractions

Figure 7 illustrates the time course (panels A–D) and steady-state (panels E–H) cell responses to instantaneous application of 20 and 100 nM [ISO], where the former is roughly half-maximally activating for most of the PKA targets. As previously shown experimentally [73] and in models [49], we observed a rise of Ca^{2+} transient amplitude and force to a peak that subsided to a slightly lower steady state level during maintained ISO exposure. The secondary sag from the maximum was concurrent with the gradual decline in $[Na^+]_i$ which is more evident at higher [ISO]. Notably, APD rapidly prolonged upon ISO (due to faster enhancement of I_{CaL} vs. I_{Ks} [46]), and subsequently shortened to a variable extent. APD shortening was less marked at higher [ISO], in part because the lower $[Na^+]_i$ drives smaller outward I_{NKA} (repolarizing) compared to 100 nM [ISO]. There is also higher Na^+ influx rate at higher [ISO]. That is because the Ca^{2+} influx and transients are larger, and in the steady state that greater Ca^{2+} influx must be balanced by greater Ca^{2+} efflux via NCX, resulting in greater Na^+ influx.

4. Discussion

We incorporated a new contractile model into a robust electrophysiological, Ca^{2+} handling, and β-AS signaling myocyte model [25, 29]. This provides a new quantitative framework to dynamically study complex interactions of β-AS effects on Ca^{2+} transient, AP and contractile properties. This allowed us to start to clarify unresolved questions about the interaction of altered XB Ca^{2+} sensitivity and XB cycling rate during β-AS in ventricular myocytes. This may also provide a useful resource for other investigators for related studies (the model is freely available).

The contractile model exhibited appropriate fundamental mechanical properties with respect to experimental data (Figs. 2–4). This includes asymmetric XB detachment (which improved fit to experimental afterloaded contraction kinetics), force-$[Ca^{2+}]_i$ relationship, frequency-dependence of stiffness, force-velocity curves and kinetic responses to abrupt stretch and release-stretch protocols. These properties and the effects of PKA were validated against critical experimental results, including data from mice with either non-phosphorylatable TnI or MyBP-C, to help analyze relative roles of XBCa and XBcy (as well as TnI and MyBP-C) in the response of twitch isometric and isotonic contractions. When embedded in a well-established electrophysiology/Ca^{2+} handling/signaling model [25, 29] the composite model produced normal APs, Ca^{2+} transients and isometric and isotonic contractions, as well as ISO responses for each.

4.1 Model assumptions

Three key changes were incorporated into our prior 6-element Ca^{2+} kinetic model [37]. First, we simplified this to a recently used 5-element version [74]. Because [TS~] in the original model, which was in the transition from TS* to TS (weak XB, Ca^{2+}-free), was <5% of the total attached XBs, the irreversible pathway from TS* to TS was combined into a

single step (eliminating TS˜; Fig. 1C). Second, we changed the velocity-dependent detachment function from a symmetrical to an asymmetrical function, a behaviour originally postulated by Huxley [42]. Third, we changed the sarcomere length-dependent lattice spacing effect on the rate function g_d from a parabolic description to an exponential representation [74], better accounting for g_d changes at any L. These changes preserved results from the previous model [37] (<10% difference in index values of F_b-$[Ca^{2+}]i$, stiffness-frequency and F_m-velocity, not shown). The newer model here has fewer differential equations and improved simulation of afterloaded contractions.

Incorporating the contractile model into the Soltis-Saucerman model [29] allowed replacing the passive Ca^{2+}-buffering by TnC with the bi-directionally coupled Ca^{2+}-XB model (Fig. 1C). Thus, length-dependent force generation is coupled to Ca^{2+} kinetics, and incorporates cooperativity between nearest-neighbor troponin complexes (within a TS). This coupling also provides inherent feedback from length and force to Ca^{2+} binding (and cytosolic buffering) by influencing transitions between states that have different Ca^{2+} affinity. Moreover, the model reproduces the classical observation [75] that abrupt shortening step during the AP causes release of Ca^{2+} from myofilaments due to the length-dependent decrease in Ca^{2+} affinity (Fig. S7). The ISO-induced reduction in TnC Ca^{2+} affinity also reduces myofilament Ca^{2+} binding, and allows peak $[Ca^{2+}]i$ to reach a significantly higher level for almost the same amount of Ca^{2+} supplied by ion channels (Fig. 6B). Indeed, a potentially surprising emergent result from the model was that changes in cytosolic (or myofilament) Ca^{2+} buffering alone had almost no effect on the AP shape, ionic currents or Ca^{2+} release and extrusion function. As discussed above, this is because the cleft and Sub-SL regions (where all Ca^{2+} transporters and channels are located) are partially isolated from the cytosolic buffering. Also the most rapid changes in $[Ca^{2+}]_{CL}$ and $[Ca^{2+}]_{SL}$, which drive current changes, occur very early in the AP, and although high $[Ca^{2+}]_i$ may reduce inward I_{CaL} in the Sub-SL, it also increases inward I_{NCX} eliminating Ca^{2+}. This raises the intriguing possibility that therapeutic approaches aimed at selective alteration of cytoplasmic buffering to accelerate twitch $[Ca^{2+}]_i$ decline [76], may have relatively modest effects on the cardiac AP and arrhythmias. This, of course, is fundamentally different for primary changes in ICaL or SR Ca^{2+} release, which will have large and relatively proportional effects on Ca^{2+}-dependent currents, their electrophysiological consequences and on contractile properties (apparent in the ISO cases in Fig. 6 and Table 4).

The model characterizes the separate effect of β-AS on TnI and MyBP-C as independent changes in the Ca^{2+} kinetic parameters involving XBCa and XBcy, respectively. This assumption was based on data suggesting relative dominance of PKA-dependent TnI phosphorylation on XBCa and of MyBP-C phosphorylation on XBcy [20, 21]. However, the exclusivity of this target-function arrangement is not universally accepted. Although emerging evidence suggests that MyBP-C may be primarily responsible for changes in XBcy in response to phosphorylation [21, 22, 77, 78] it may also contribute to XBCa when regulatory light chain phosphorylation has been reduced [22], or when basal levels of phosphorylation are decreased by propranolol pretreatment [23]. Conversely, there is also some evidence that TnI phosphorylation by PKA is critical for XBcy effects [18]. While our model is consistent with a separate influence of β-AS on XBCa and XBcy, the model itself

may be instrumental in further elucidation of the functional interaction between TnI and MyBP-C phosphorylation sites.

ISO effects on ion currents and Ca^{2+} transport were mostly as in the Soltis-Saucerman model [29], with modifications based on experimental data and our recent theoretical studies [46, 52] and indicated in Methods. In addition, $I_{Cl(Ca)}$ was slightly enhanced by ISO [53], whereas I_{NCX} properties were not altered [79, 80], despite earlier data suggesting such modulation [81]. The set of myofilament parameters and ISO-induced shifts was adequate to mimic experimental findings in wild type and transgenic mice with non-phosphorylatable TnI or MyBP-C. That enabled predictions of relative XBCa and XBcy participation in isometric and isotonic twitch behavior. Although some relative shifts were inferred from transgenic mice, these were imbedded in the Soltis-Saucerman model that is based on the Shannon-Bers rabbit myocyte framework. This was motivated, in part, by the likely more direct extension to the human ventricular myocyte regarding electrophysiology and Ca^{2+} handling [82]. The model creates a template that will allow newer data to be added to improve its accuracy for both rabbit and human tissue. Also, our model allows simulating variable degrees of β-AS, as demonstrated in Fig. 7.

4.2 β-AS effects on contractility

We systematically switched off the β-AS effect from each of 11 individual targets to analyze their relative impact on contractility. Preventing β-AS effects on I_{CaL} or PLB limited Ca^{2+} transients and contractile responses in parallel, while blocking PLM and K^+ channel (I_{Ks}) effects enhanced Ca^{2+} and inotropy. These results are all consistent with the expected effects of these individual targets. But the integrated model here allows a relative assessment of the impacts of each process to β-AS induced inotropy and lusitropy. Four other ion transporters (RyR, I_{Kr}, CFTR, $I_{Cl}(Ca)$) are modulated by PKA effects in the model, but their net effects on Ca^{2+} transients and contraction were minimal.

The satisfactory simulation of F_b-$[Ca^{2+}]_i$ relationships [18, 20, 83], release-restretch [20, 21] and length step [23] experiments at fixed $[Ca^{2+}]_i$, demonstrates the adequate behavior of the present model. These results enabled the dissection of the ISO twitch response (Table 4 and Fig. 6) to understand the separate role of XBCa and XBcy on contractility. Results of Ca^{2+} transient and isometric and isotonic twitches suggest that enhanced XBcy is essential to explain the twitch inotropic response, and without that the larger Ca^{2+} transient appears only able to offset the intrinsic negative inotropic effect of ISO-induced reduced myofilament Ca^{2+} sensitivity (XBCa). The larger and faster Ca^{2+} fluxes are also essential, because without them ISO would have a slightly negative or a reduced inotropic effect for isometric and isotonic contractions, respectively (Table 4; ISO-Cytofl). The absence of both XBCa and XBcy effects does not prevent inotropic and lusitropic effects of ISO, due to the larger and faster Ca^{2+} transients (although the lack of XBcy greatly limits inotropy in the isotonic case). The reduced XBCa contributes to faster relaxation and shorter time to peak, and the enhanced XBcy amplifies the inotropic effect (but also slows kinetics). Notably, the XBcy effect is especially critical for isotonic contraction during sarcomere shortening, because without that ISO reduces shortening vs. control despite the much larger Ca^{2+} transients. Looking at this another way, the ISO-induced increase in Ca^{2+} transient offsets the reduced

XBCa, resulting in little difference in force or shortening vs. control, whereas enhanced XBcy drives the net enhancement of contraction.

For isometric force, enhanced XBcy and Ca^{2+} cycling contribute roughly equally to force development, whereas for isotonic contraction enhanced XBcy is more critical than enhanced Ca^{2+} cycling for maximal shortening. With respect to kinetics, the situation differs. Both faster Ca^{2+} kinetics and reduced XBCa contribute to the shorter time to peak and faster relaxation, and both work against the enhanced XBcy (which by itself slows relaxation).

4.3 Limitations

Our contraction model is based on cardiac data from multiple species (frog, guinea pig, rabbit, ferret and cat), whereas the ionic and Ca^{2+} handling model is based more explicitly on rabbit data. In both cases temperature-dependent parameters were adapted to 37°C [25, 37]. Ideally, all model parameters should be derived from rabbit at 37°C. However, as is often the case in model development [84], there is limited rabbit data at 37°C to constrain the mechanical model. So, we used available data from various species, including seminal rabbit data [35, 37] and from genetically modified mice, which are of unique value in distinguishing effects of TnI and MyBP-C phosphorylation sites. We think the model is a very good approximation, but this necessary compromise is a model limitation. Of course the model can be further tuned as additional relevant data becomes available with respect to any of the model assumptions.

The model also includes CaMKII signaling, and there is known to be some cross-talk between β-AS and CaMKII signaling. We tested how much CaMKII effects might contribute to the acute ISO effects reported here (Fig. S8 vs. Fig. 7). Turning off CaMKII effects had only slight effects on acute ISO effects, so the ISO effects we report here are almost entirely PKA-dependent. That agrees with data showing that ISO-induced inotropic and lusitropic effects are preserved in CaMKIIδ knockout mice [85].

4.4 Conclusions

We have developed a useful model to study the interplay of mechanical, Ca^{2+} handling and electrophysiological properties of cardiac myocytes. Here we have used it to improve our understanding of how XBCa and XBcy effects of ISO interact with each other during both isometric and isotonic contractions. Coupling the contractile and Ca^{2+}-AP models allowed us to study how ion channel and Ca^{2+} changes influence contraction dynamically, and also how the contractile process feeds back to influence $[Ca^{2+}]_i$. An emergent finding was that changes in myofilament Ca^{2+} buffering can influence $[Ca^{2+}]_i$, but at the same time have little direct impact on ionic currents and the AP shape. Both increased XBcy and Ca^{2+} transients contribute to enhanced contractility during β-AS isometric systole, whereas XBcy may be more critical during cardiac ejection when sarcomere shortening occurs. The model may also be useful for both further study of these AP-Ca^{2+}-XBCa-XBcy interactions and incorporation into multicellular or intact heart models.

Supplementary Material

Refer to Web version on PubMed Central for supplementary material.

Acknowledgments

This research was supported by ANPCyT PICT08–0340-grant (JAN, ECL), by a Postdoctoral fellowship from the American Heart Association (SM), and NIH grants R01–HL096819 (AVG), R01–HL105242 and R37–HL30077 (DB).

Abbreviations

AP	Action potential
APD	AP duration
CaMKII	Ca^{2+}/calmodulin-dependent protein kinase II
E–C	Excitation-contraction
F_m	Muscle force
I_{CaL}	L-type Ca^{2+} channel current
I_{CFTR}	CFTR-mediated Cl^- current
$I_{Cl(Ca)}$	Ca^{2+}-dependent Cl^- current
I_{Kr}	Rapid delayed rectifier K^+ current
I_{Ks}	Slow delayed rectifier K^+ current
I_{Na}	Fast Na^+ current
I_{NCX}	Na^+-Ca^{2+} exchanger current
I_{NKA}	Na^+-K^+-ATPase current
ISO	Isoproterenol
ISO-Cytofl	ISO effect without β-AS on parameters involved in cytosolic fluxes
ISO-titin	ISO effect without β-AS on parameters involved in titin
ISO-XBCa	ISO effect without β-AS on parameters involved in XBCa
ISO-XBCa-XBcy	ISO effect without β-AS on parameters in XBCa and XBcy
ISO-XBcy	ISO effect without β-AS on parameters involved in XBcy
k_{df}	Rate of force redevelopment (response to a length step)
k_{rel}	Rate of force decay
k_{tr}	Rate of force redevelopment (response to a length pulse)
L_m	Muscle length
MyBP-C	Myosin binding protein-C
NCX	Na^+-Ca^{2+} exchanger

NKA	Na^+-K^+-ATPase
PKA	Protein kinase A
PLB	Phospholamban
PLM	Phospholemman
RyR	Ryanodine receptor
SERCA	SR Ca^{2+}-ATPase
SR	Sarcoplasmic reticulum
TnC	Troponin C
TnI	Troponin I
XB	Myofilament cross-bridge
XBCa	XB Ca^{2+} sensitivity
XBcy	XB cycling rate
β-AS	un β-adrenergic stimulation

References

1. McDonald TF, Pelzer S, Trautwein W, Pelzer DJ. Regulation and modulation of calcium channels in cardiac, skeletal, and smooth muscle cells. Physiol Rev. 1994; 74:365–507. [PubMed: 8171118]
2. Tsien RW, Bean BP, Hess P, Lansman JB, Nilius B, Nowycky MC. Mechanisms of calcium channel modulation by beta-adrenergic agents and dihydropyridine calcium agonists. J Mol Cell Cardiol. 1986; 18:691–710. [PubMed: 2427730]
3. Lindemann JP, Jones LR, Hathaway DR, Henry BG, Watanabe AM. beta-Adrenergic stimulation of phospholamban phosphorylation and Ca^{2+}-ATPase activity in guinea pig ventricles. The Journal of biological chemistry. 1983; 258:464–71. [PubMed: 6217205]
4. Hunter DR, Haworth RA, Berkoff HA. Modulation of cellular calcium stores in the perfused rat heart by isoproterenol and ryanodine. Circulation research. 1983; 53:703–12. [PubMed: 6414734]
5. Shannon TR, Ginsburg KS, Bers DM. Quantitative assessment of the SR Ca^{2+} leak-load relationship. Circulation research. 2002; 91:594–600. [PubMed: 12364387]
6. Shan J, Kushnir A, Betzenhauser MJ, Reiken S, Li J, Lehnart SE, et al. Phosphorylation of the ryanodine receptor mediates the cardiac fight or flight response in mice. The Journal of clinical investigation. 2010; 120:4388–98. [PubMed: 21099118]
7. Curran J, Hinton MJ, Rios E, Bers DM, Shannon TR. Beta-adrenergic enhancement of sarcoplasmic reticulum calcium leak in cardiac myocytes is mediated by calcium/calmodulin-dependent protein kinase. Circulation research. 2007; 100:391–8. [PubMed: 17234966]
8. Li Y, Kranias EG, Mignery GA, Bers DM. Protein kinase A phosphorylation of the ryanodine receptor does not affect calcium sparks in mouse ventricular myocytes. Circulation research. 2002; 90:309–16. [PubMed: 11861420]
9. Bers DM. Ryanodine receptor S2808 phosphorylation in heart failure: smoking gun or red herring. Circulation research. 2012; 110:796–9. [PubMed: 22427320]
10. Curran J, Tang L, Roof SR, Velmurugan S, Millard A, Shonts S, et al. Nitric oxide-dependent activation of CaMKII increases diastolic sarcoplasmic reticulum calcium release in cardiac myocytes in response to adrenergic stimulation. PloS one. 2014; 9:e87495. [PubMed: 24498331]
11. Pereira L, Cheng H, Lao DH, Na L, van Oort RJ, Brown JH, et al. Epac2 mediates cardiac beta1-adrenergic-dependent sarcoplasmic reticulum Ca^{2+} leak and arrhythmia. Circulation. 2013; 127:913–22. [PubMed: 23363625]

12. Sanguinetti MC, Jurkiewicz NK, Scott A, Siegl PK. Isoproterenol antagonizes prolongation of refractory period by the class III antiarrhythmic agent E-4031 in guinea pig myocytes. Mechanism of action. Circulation research. 1991; 68:77–84. [PubMed: 1984874]
13. Koumi S, Backer CL, Arentzen CE, Sato R. beta-Adrenergic modulation of the inwardly rectifying potassium channel in isolated human ventricular myocytes. Alteration in channel response to beta-adrenergic stimulation in failing human hearts. The Journal of clinical investigation. 1995; 96:2870–81. [PubMed: 8675658]
14. Li L, Desantiago J, Chu G, Kranias EG, Bers DM. Phosphorylation of phospholamban and troponin I in betaadrenergic-induced acceleration of cardiac relaxation. Am J Physiol Heart Circ Physiol. 2000; 278:H769–79. [PubMed: 10710345]
15. Sadayappan S, Gulick J, Klevitsky R, Lorenz JN, Sargent M, Molkentin JD, et al. Cardiac myosin binding protein-C phosphorylation in a {beta}-myosin heavy chain background. Circulation. 2009; 119:1253–62. [PubMed: 19237661]
16. Kranias EG, Garvey JL, Srivastava RD, Solaro RJ. Phosphorylation and functional modifications of sarcoplasmic reticulum and myofibrils in isolated rabbit hearts stimulated with isoprenaline. The Biochemical journal. 1985; 226:113–21. [PubMed: 3156585]
17. Garvey JL, Kranias EG, Solaro RJ. Phosphorylation of C-protein, troponin I and phospholamban in isolated rabbit hearts. The Biochemical journal. 1988; 249:709–14. [PubMed: 2895634]
18. Kentish JC, McCloskey DT, Layland J, Palmer S, Leiden JM, Martin AF, et al. Phosphorylation of troponin I by protein kinase A accelerates relaxation and crossbridge cycle kinetics in mouse ventricular muscle. Circulation research. 2001; 88:1059–65. [PubMed: 11375276]
19. Layland J, Solaro RJ, Shah AM. Regulation of cardiac contractile function by troponin I phosphorylation. Cardiovascular research. 2005; 66:12–21. [PubMed: 15769444]
20. Tong CW, Stelzer JE, Greaser ML, Powers PA, Moss RL. Acceleration of crossbridge kinetics by protein kinase A phosphorylation of cardiac myosin binding protein C modulates cardiac function. Circulation research. 2008; 103:974–82. [PubMed: 18802026]
21. Stelzer JE, Patel JR, Walker JW, Moss RL. Differential roles of cardiac myosin-binding protein C and cardiac troponin I in the myofibrillar force responses to protein kinase A phosphorylation. Circulation research. 2007; 101:503–11. [PubMed: 17641226]
22. Chen PP, Patel JR, Rybakova IN, Walker JW, Moss RL. Protein kinase A-induced myofilament desensitization to Ca^{2+} as a result of phosphorylation of cardiac myosin-binding protein C. The Journal of general physiology. 2010; 136:615–27. [PubMed: 21115695]
23. Bardswell SC, Cuello F, Rowland AJ, Sadayappan S, Robbins J, Gautel M, et al. Distinct sarcomeric substrates are responsible for protein kinase D-mediated regulation of cardiac myofilament Ca^{2+} sensitivity and crossbridge cycling. The Journal of biological chemistry. 2010; 285:5674–82. [PubMed: 20018870]
24. Puglisi JL, Wang F, Bers DM. Modeling the isolated cardiac myocyte. Prog Biophys Mol Biol. 2004; 85:163–78. [PubMed: 15142742]
25. Shannon TR, Wang F, Puglisi J, Weber C, Bers DM. A mathematical treatment of integrated Ca dynamics within the ventricular myocyte. Biophys J. 2004; 87:3351–71. [PubMed: 15347581]
26. Nordin C, Ming Z. Computer model of current-induced early afterdepolarizations in guinea pig ventricular myocytes. Am J Physiol. 1995; 268:H2440–59. [PubMed: 7611496]
27. Saucerman JJ, Brunton LL, Michailova AP, McCulloch AD. Modeling beta-adrenergic control of cardiac myocyte contractility in silico. The Journal of biological chemistry. 2003; 278:47997–8003. [PubMed: 12972422]
28. Saucerman JJ, Bers DM. Calmodulin mediates differential sensitivity of CaMKII and calcineurin to local Ca^{2+} in cardiac myocytes. Biophys J. 2008; 95:4597–612. [PubMed: 18689454]
29. Soltis AR, Saucerman JJ. Synergy between CaMKII substrates and beta-adrenergic signaling in regulation of cardiac myocyte Ca^{2+} handling. Biophys J. 2010; 99:2038–47. [PubMed: 20923637]
30. Morotti S, Edwards AG, McCulloch AD, Bers DM, Grandi E. A novel computational model of mouse myocyte electrophysiology to assess the synergy between Na+ loading and CaMKII. J Physiol. 2014; 592:1181–97. [PubMed: 24421356]

31. Cortassa S, Aon MA, O'Rourke B, Jacques R, Tseng HJ, Marban E, et al. A computational model integrating electrophysiology, contraction, and mitochondrial bioenergetics in the ventricular myocyte. Biophys J. 2006; 91:1564–89. [PubMed: 16679365]
32. Crampin EJ, Smith NP. A dynamic model of excitation-contraction coupling during acidosis in cardiac ventricular myocytes. Biophys J. 2006; 90:3074–90. [PubMed: 16473911]
33. Hunter PJ, McCulloch AD, ter Keurs HE. Modelling the mechanical properties of cardiac muscle. Prog Biophys Mol Biol. 1998; 69:289–331. [PubMed: 9785944]
34. Chin L, Yue P, Feng JJ, Seow CY. Mathematical simulation of muscle cross-bridge cycle and force-velocity relationship. Biophys J. 2006; 91:3653–63. [PubMed: 16935957]
35. Peterson JN, Hunter WC, Berman MR. Estimated time course of Ca^{2+} bound to troponin C during relaxation in isolated cardiac muscle. Am J Physiol. 1991; 260:H1013–24. [PubMed: 2000960]
36. Rice JJ, Stolovitzky G, Tu Y, de Tombe PP. Ising model of cardiac thin filament activation with nearest-neighbor cooperative interactions. Biophys J. 2003; 84:897–909. [PubMed: 12547772]
37. Negroni JA, Lascano EC. Simulation of steady state and transient cardiac muscle response experiments with a Huxley-based contraction model. J Mol Cell Cardiol. 2008; 45:300–12. [PubMed: 18550079]
38. Noble D, Varghese A, Kohl P, Noble P. Improved guinea-pig ventricular cell model incorporating a diadic space, IKr and IKs, and length- and tension-dependent processes. Can J Cardiol. 1998; 14:123–34. [PubMed: 9487284]
39. Rice JJ, Wang F, Bers DM, de Tombe PP. Approximate model of cooperative activation and crossbridge cycling in cardiac muscle using ordinary differential equations. Biophys J. 2008; 95:2368–90. [PubMed: 18234826]
40. Heijman J, Volders PG, Westra RL, Rudy Y. Local control of beta-adrenergic stimulation: Effects on ventricular myocyte electrophysiology and Ca^{2+}-transient. J Mol Cell Cardiol. 2011; 50:863–71. [PubMed: 21345340]
41. Saucerman JJ, McCulloch AD. Mechanistic systems models of cell signaling networks: a case study of myocyte adrenergic regulation. Prog Biophys Mol Biol. 2004; 85:261–78. [PubMed: 15142747]
42. Huxley AF. Muscle structure and theories of contraction. Progress in biophysics and biophysical chemistry. 1957; 7:255–318. [PubMed: 13485191]
43. Negroni JA, Lascano EC. A cardiac muscle model relating sarcomere dynamics to calcium kinetics. J Mol Cell Cardiol. 1996; 28:915–29. [PubMed: 8762031]
44. Slawnych MP, Seow CY, Huxley AF, Ford LE. A program for developing a comprehensive mathematical description of the crossbridge cycle of muscle. Biophys J. 1994; 67:1669–77. [PubMed: 7819498]
45. Metzger JM, Moss RL. Shortening velocity in skinned single muscle fibers. Influence of filament lattice spacing. Biophys J. 1987; 52:127–31. [PubMed: 3607220]
46. Xie Y, Grandi E, Puglisi JL, Sato D, Bers DM. beta-adrenergic stimulation activates early afterdepolarizations transiently via kinetic mismatch of PKA targets. J Mol Cell Cardiol. 2013; 58:153–61. [PubMed: 23481579]
47. Liu GX, Choi BR, Ziv O, Li W, de Lange E, Qu Z, et al. Differential conditions for early afterdepolarizations and triggered activity in cardiomyocytes derived from transgenic LQT1 and LQT2 rabbits. J Physiol. 2012; 590:1171–80. [PubMed: 22183728]
48. Despa S, Bossuyt J, Han F, Ginsburg KS, Jia LG, Kutchai H, et al. Phospholemman-phosphorylation mediates the beta-adrenergic effects on Na/K pump function in cardiac myocytes. Circulation research. 2005; 97:252–9. [PubMed: 16002746]
49. Yang JH, Saucerman JJ. Phospholemman is a negative feed-forward regulator of Ca^{2+} in beta-adrenergic signaling, accelerating beta-adrenergic inotropy. J Mol Cell Cardiol. 2012; 52:1048–55. [PubMed: 22289214]
50. Moreno JD, Yang PC, Bankston JR, Grandi E, Bers DM, Kass RS, et al. Ranolazine for congenital and acquired late INa-linked arrhythmias: in silico pharmacological screening. Circulation research. 2013; 113:e50–61. [PubMed: 23897695]

51. Harmati G, Banyasz T, Barandi L, Szentandrassy N, Horvath B, Szabo G, et al. Effects of beta-adrenoceptor stimulation on delayed rectifier K(+) currents in canine ventricular cardiomyocytes. British journal of pharmacology. 2011; 162:890–6. [PubMed: 20973780]
52. Xie Y, Grandi E, Bers DM, Sato D. How does beta-adrenergic signalling affect the transitions from ventricular tachycardia to ventricular fibrillation? Europace: European pacing, arrhythmias, and cardiac electrophysiology: journal of the working groups on cardiac pacing, arrhythmias, and cardiac cellular electrophysiology of the European Society of Cardiology. 2014; 16:452–7.
53. Zygmunt AC, Gibbons WR. Calcium-activated chloride current in rabbit ventricular myocytes. Circulation research. 1991; 68:424–37. [PubMed: 1991347]
54. Kruger M, Linke WA. Titin-based mechanical signalling in normal and failing myocardium. J Mol Cell Cardiol. 2009; 46:490–8. [PubMed: 19639676]
55. Robertson SP, Johnson JD, Holroyde MJ, Kranias EG, Potter JD, Solaro RJ. The effect of troponin I phosphorylation on the Ca^{2+}-binding properties of the Ca^{2+}-regulatory site of bovine cardiac troponin. The Journal of biological chemistry. 1982; 257:260–3. [PubMed: 7053370]
56. Fukuda N, Wu Y, Nair P, Granzier HL. Phosphorylation of titin modulates passive stiffness of cardiac muscle in a titin isoform-dependent manner. The Journal of general physiology. 2005; 125:257–71. [PubMed: 15738048]
57. Gao WD, Backx PH, Azan-Backx M, Marban E. Myofilament Ca^{2+} sensitivity in intact versus skinned rat ventricular muscle. Circulation research. 1994; 74:408–15. [PubMed: 8118949]
58. Dobesh DP, Konhilas JP, de Tombe PP. Cooperative activation in cardiac muscle: impact of sarcomere length. Am J Physiol Heart Circ Physiol. 2002; 282:H1055–62. [PubMed: 11834504]
59. Okazaki O, Suda N, Hongo K, Konishi M, Kurihara S. Modulation of Ca^{2+} transients and contractile properties by beta-adrenoceptor stimulation in ferret ventricular muscles. J Physiol. 1990; 423:221–40. [PubMed: 1696985]
60. Varian KD, Raman S, Janssen PM. Measurement of myofilament calcium sensitivity at physiological temperature in intact cardiac trabeculae. Am J Physiol Heart Circ Physiol. 2006; 290:H2092–7. [PubMed: 16603708]
61. Shibata T, Hunter WC, Yang A, Sagawa K. Dynamic stiffness measured in central segment of excised rabbit papillary muscles during barium contracture. Circulation research. 1987; 60:756–69. [PubMed: 3594749]
62. Hongo K, Tanaka E, Kurihara S. Alterations in contractile properties and Ca^{2+} transients by beta- and muscarinic receptor stimulation in ferret myocardium. J Physiol. 1993; 461:167–84. [PubMed: 8394423]
63. Herron TJ, Korte FS, McDonald KS. Power output is increased after phosphorylation of myofibrillar proteins in rat skinned cardiac myocytes. Circulation research. 2001; 89:1184–90. [PubMed: 11739284]
64. Sonnenblick EH. Force-velocity relations in mammalian heart muscle. Am J Physiol. 1962; 202:931–9. [PubMed: 13915199]
65. Vannier C, Chevassus H, Vassort G. Ca-dependence of isometric force kinetics in single skinned ventricular cardiomyocytes from rats. Cardiovascular research. 1996; 32:580–6. [PubMed: 8881518]
66. Patel JR, Fitzsimons DP, Buck SH, Muthuchamy M, Wieczorek DF, Moss RL. PKA accelerates rate of force development in murine skinned myocardium expressing alpha- or beta-tropomyosin. Am J Physiol Heart Circ Physiol. 2001; 280:H2732–9. [PubMed: 11356630]
67. Ng GA, Mantravadi R, Walker WH, Ortin WG, Choi BR, de Groat W, et al. Sympathetic nerve stimulation produces spatial heterogeneities of action potential restitution. Heart rhythm: the official journal of the Heart Rhythm Society. 2009; 6:696–706. [PubMed: 19389655]
68. Malfatto G, Rocchetti M, Zaza A. The role of the autonomic system in rate-dependent repolarization changes. Heart rhythm: the official journal of the Heart Rhythm Society. 2010; 7:1700–3. [PubMed: 20621621]
69. Bers, DM. Excitation-contraction coupling and cardiac contractile force. The Netherlands: Kluwer Academic Publishers; 2001.

70. Briston SJ, Dibb KM, Solaro RJ, Eisner DA, Trafford AW. Balanced changes in Ca buffering by SERCA and troponin contribute to Ca handling during beta-adrenergic stimulation in cardiac myocytes. Cardiovascular research. 2014; 104:347–54. [PubMed: 25183792]
71. Layland J, Kentish JC. Myofilament-based relaxant effect of isoprenaline revealed during work-loop contractions in rat cardiac trabeculae. J Physiol. 2002; 544:171–82. [PubMed: 12356890]
72. Spurgeon HA, Stern MD, Baartz G, Raffaeli S, Hansford RG, Talo A, et al. Simultaneous measurement of Ca^{2+}, contraction, and potential in cardiac myocytes. Am J Physiol. 1990; 258:H574–86. [PubMed: 2309919]
73. Despa S, Tucker AL, Bers DM. Phospholemman-mediated activation of Na/K-ATPase limits [Na]i and inotropic state during beta-adrenergic stimulation in mouse ventricular myocytes. Circulation. 2008; 117:1849–55. [PubMed: 18362230]
74. Lascano EC, Said M, Vittone L, Mattiazzi A, Mundina-Weilenmann C, Negroni JA. Role of CaMKII in post acidosis arrhythmias: *a simulation study using a human myocyte model*. J Mol Cell Cardiol. 2013; 60:172–83. [PubMed: 23624090]
75. Allen DG, Kurihara S. The effects of muscle length on intracellular calcium transients in mammalian cardiac muscle. J Physiol. 1982; 327:79–94. [PubMed: 7120151]
76. Wang W, Barnabei MS, Asp ML, Heinis FI, Arden E, Davis J, et al. Noncanonical EF-hand motif strategically delays Ca^{2+} buffering to enhance cardiac performance. Nature medicine. 2013; 19:305–12.
77. Colson BA, Patel JR, Chen PP, Bekyarova T, Abdalla MI, Tong CW, et al. Myosin binding protein-C phosphorylation is the principal mediator of protein kinase A effects on thick filament structure in myocardium. J Mol Cell Cardiol. 2012; 53:609–16. [PubMed: 22850286]
78. Mamidi R, Gollapudi SK, Mallampalli SL, Chandra M. Alanine or aspartic acid substitutions at serine23/24 of cardiac troponin I decrease thin filament activation, with no effect on crossbridge detachment kinetics. Archives of biochemistry and biophysics. 2012; 525:1–8. [PubMed: 22684024]
79. Ginsburg KS, Bers DM. Isoproterenol does not enhance Ca-dependent Na/Ca exchange current in intact rabbit ventricular myocytes. J Mol Cell Cardiol. 2005; 39:972–81. [PubMed: 16242149]
80. Lin X, Jo H, Sakakibara Y, Tambara K, Kim B, Komeda M, et al. Beta-adrenergic stimulation does not activate Na^{+}/Ca^{2+} exchange current in guinea pig, mouse, and rat ventricular myocytes. American journal of physiology Cell physiology. 2006; 290:C601–8. [PubMed: 16207789]
81. Ruknudin A, He S, Lederer WJ, Schulze DH. Functional differences between cardiac and renal isoforms of the rat Na^{+}-Ca^{2+} exchanger NCX1 expressed in Xenopus oocytes. J Physiol. 2000; 529(Pt 3):599–610. [PubMed: 11118492]
82. Grandi E, Pasqualini FS, Bers DM. A novel computational model of the human ventricular action potential and Ca transient. J Mol Cell Cardiol. 2010; 48:112–21. [PubMed: 19835882]
83. Ramirez-Correa GA, Cortassa S, Stanley B, Gao WD, Murphy AM. Calcium sensitivity, force frequency relationship and cardiac troponin I: critical role of PKA and PKC phosphorylation sites. J Mol Cell Cardiol. 2010; 48:943–53. [PubMed: 20083117]
84. Niederer SA, Smith NP. At the heart of computational modelling. J Physiol. 2012; 590:1331–8. [PubMed: 22271869]
85. Neef S, Sag CM, Daut M, Baumer H, Grefe C, El-Armouche A, et al. While systolic cardiomyocyte function is preserved, diastolic myocyte function and recovery from acidosis are impaired in CaMKIIdelta-KO mice. J Mol Cell Cardiol. 2013; 59:107–16. [PubMed: 23473775]
86. Brutsaert DL, de Clerck NM, Goethals MA, Housmans PR. Relaxation of ventricular cardiac muscle. J Physiol. 1978; 283:469–80. [PubMed: 722587]

Highlights

- β-AS effects on cardiac contraction are analyzed with a new computer model.
- The model reproduces a range of experiments involving force and length changes.
- Impact of PKA targets to ®-AS effects on AP, Ca2+ and contraction is studied.
- ICa, PLB, PLM and I_{Ks} effects dominate in the ®-AS increase in Ca2+ transients.
- Increased XBcy compensates for lower myofilament Ca2+ sensitivity during inotropy.

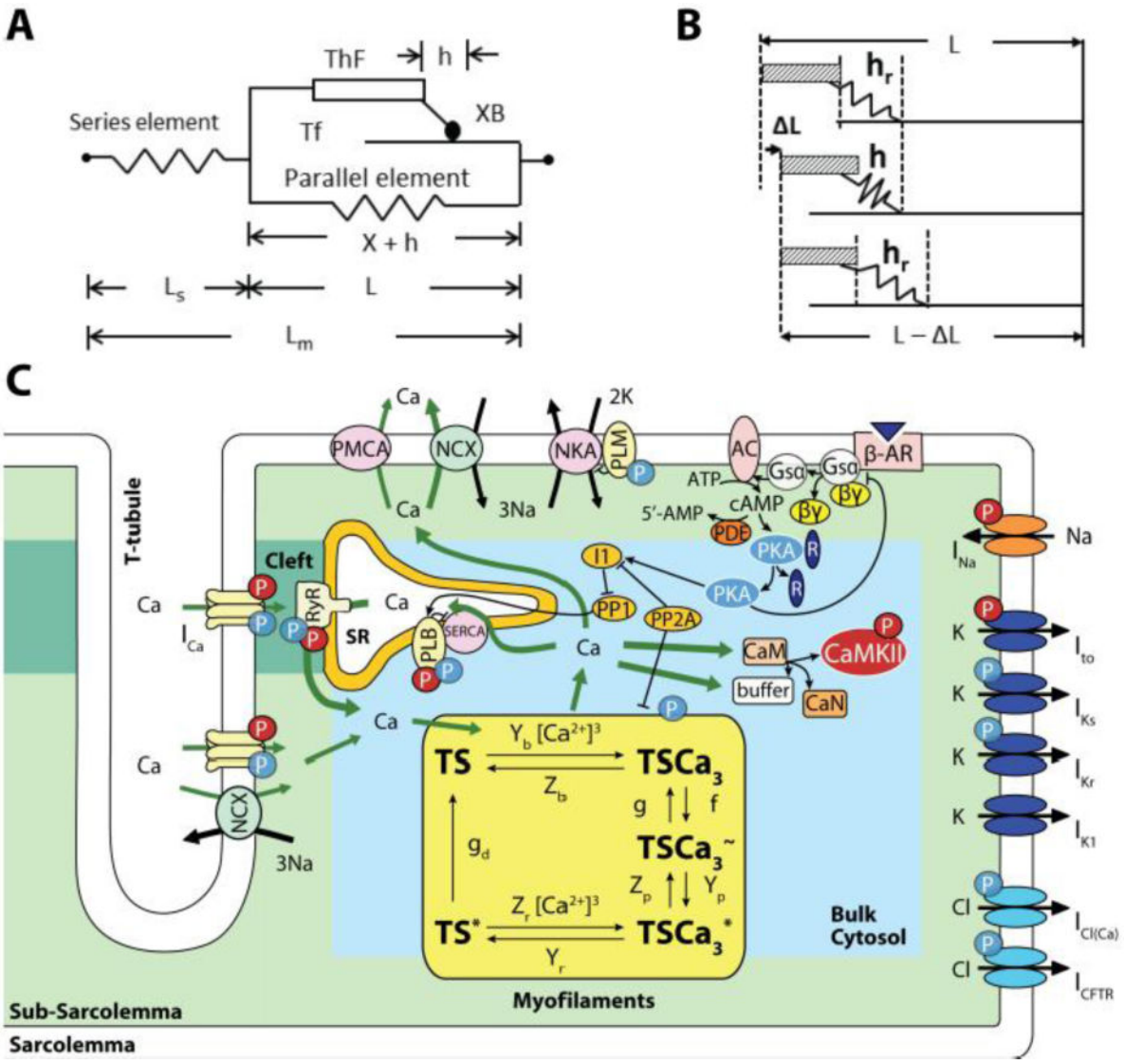

Figure 1.

Model. **A:** Constitutive muscle unit, consisting of half-sarcomere length (L) composed of thick (ThF) and thin (Tf) filaments in parallel with an elastic element. The equivalent cross-bride (XB) representing all attached cross-bridges is part of the ThF. It attaches to the Tf by the mobile end of its elastic structure, with h elongation, defining an inextensible half-sarcomere length X = L − h. A series elastic element with length L_s accounts for compliant muscle ends and together with L make up total muscle length (L_m). **B:** Cross-bridge dynamics showing steadystate XB elongation (h_r), its decrease due to ΔL and later return to h_r at shorter half-sarcomere length (L-ΔL). **C:** Four compartment myocyte model: Bulk Cytosol, Cleft, sarcoplasmic reticulum (SR) and subsarcolemmal space (Sub-SL) [25, 29] with ion currents as described by these authors. This model is coupled to the myofilament force development model consisting of 5-state troponin systems (TS) with Ca^{2+} binding. Each TS is composed of three adjacent troponin–tropomyosin regulatory units able to act cooperatively to bind Ca^{2+} in three successive steps. Troponin systems are: free TS; Ca^{2+}

bound to TS without attached XBs ($TSCa_3$), Ca^{2+} bound to TS with attached XBs in the weak state ($TSCa_3$~), Ca^{2+} bound to TS with attached XBs in the power state ($TSCa_3$*), and TS without Ca^{2+} with attached XBs in the power state (TS*). Baseline mechanical parameters and all changes used for ISO are in Table 1.

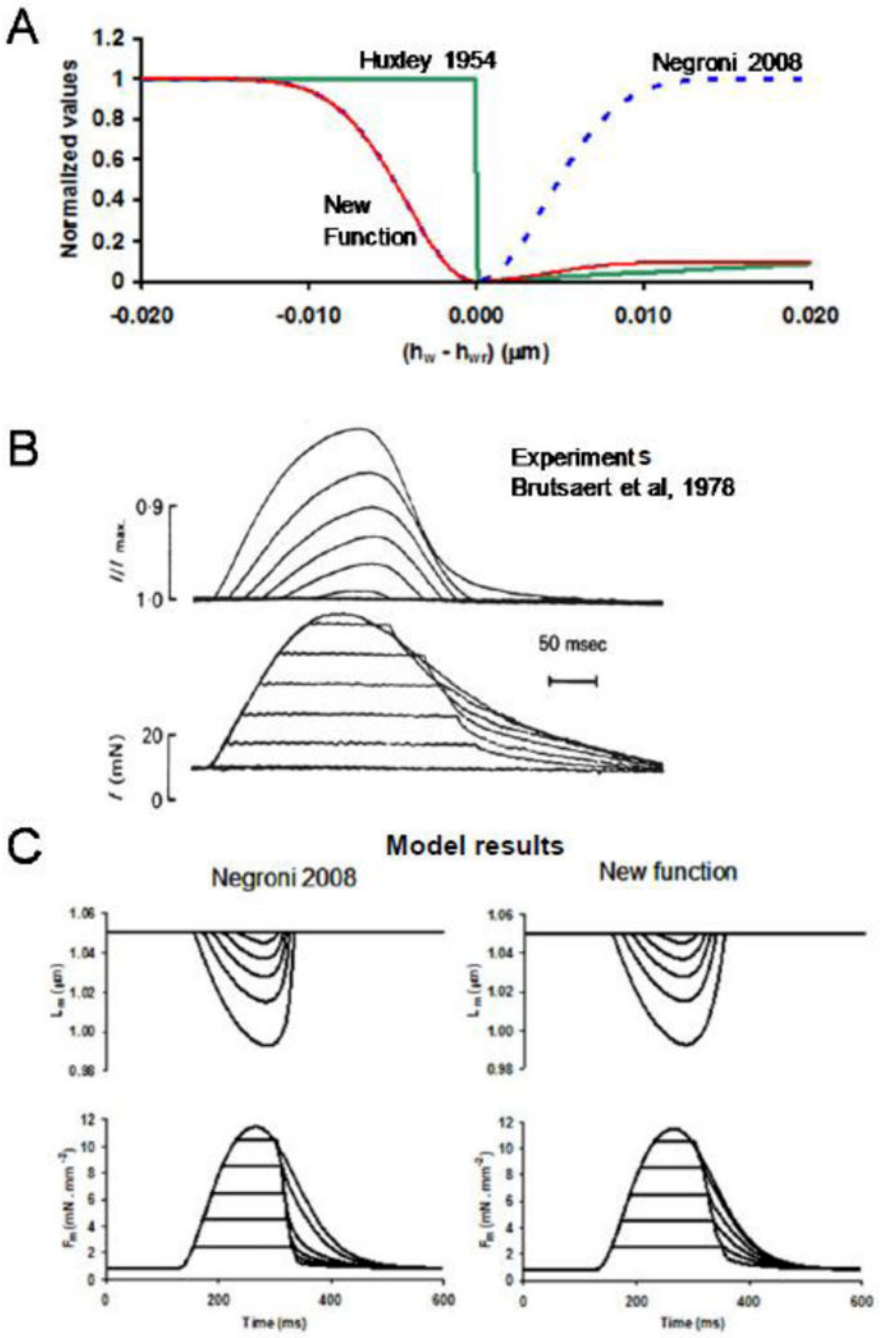

Figure 2.

Asymmetrical detachment function validated by its effect on afterloaded contractions. **A:** Normalized detachment as a function of the difference between weak (h_w) and steady state weak (h_{wr}) XB length. The previous symmetrical detachment function [37] based on the proposition of Slawnych *et al.* [44] was corrected, incorporating the asymmetry (New function) postulated by Huxley [42]. **B:** Experimental afterloaded contractions from Brutsaert *et al.* [86]. **C:** Simulation of myocyte afterloaded contractions with Negroni *et al.*

detachment function [37] and the new detachment function, resembling more accurately the experimental reports.

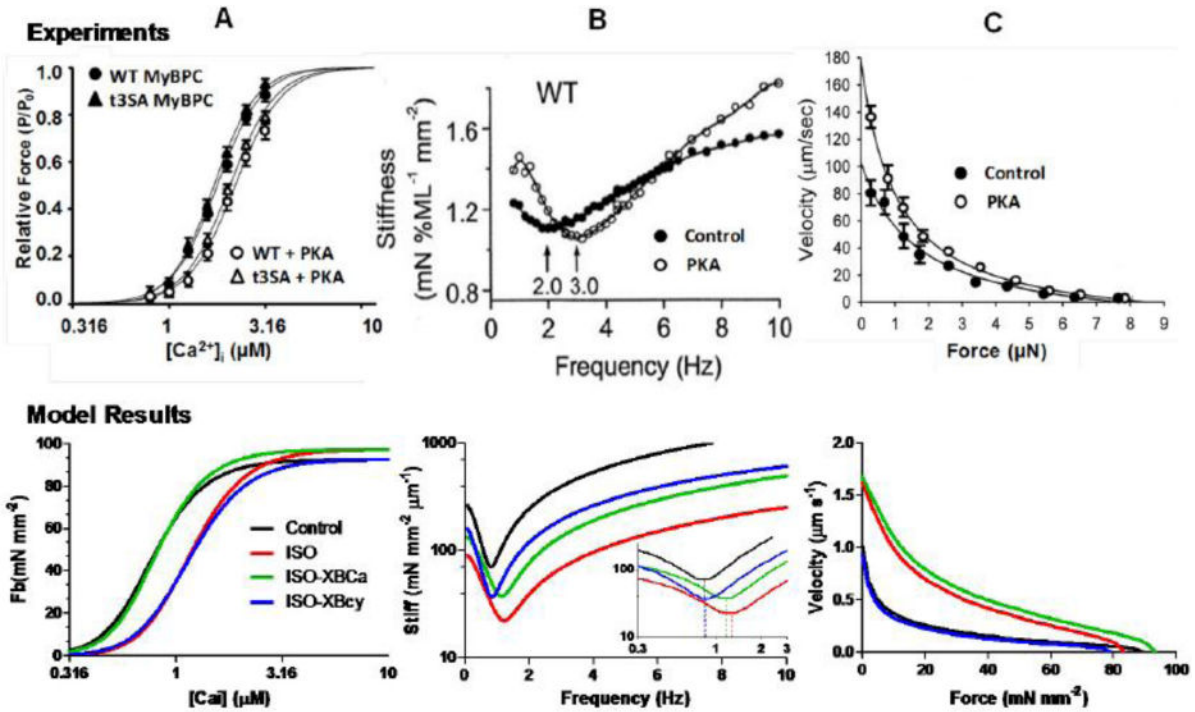

Figure 3.

Experimentally reported (upper panels) and model simulated (lower panels) contractile response at fixed $[Ca^{2+}]_i$. **A:** Model simulated XB force (F_b) – $[Ca^{2+}]_i$ relationships depict rightward shift in ISO (100 nM) and ISO-XBcy, but comparable to control in ISO-XBCa, as seen in experimental results with PKA in WT or non phosphorylatable MyBPC (cMyoBP-C(t3SA)) mice [20]. **B:** Stiffness-frequency relationship simulations exhibit a shift of minimum stiffness towards higher frequency in ISO (see inset), as seen in experimental data with ISO in WT mice [18]. This effect is partially abolished in ISO-XBCa, though the effect is less than in TG experiments, and is eliminated in ISO-XBcy. **C:** force-velocity curves built from isotonic shortening velocities at imposed loads starting at isometric force (L_m = 1.05 μm). Shifts with ISO are comparable to experimental responses [63]. ISO-XBCa was similar to ISO and ISO-XBcy analogous to control, suggesting force-velocity dependence mainly on XBcy (see Table 3 for simulation numerical values).

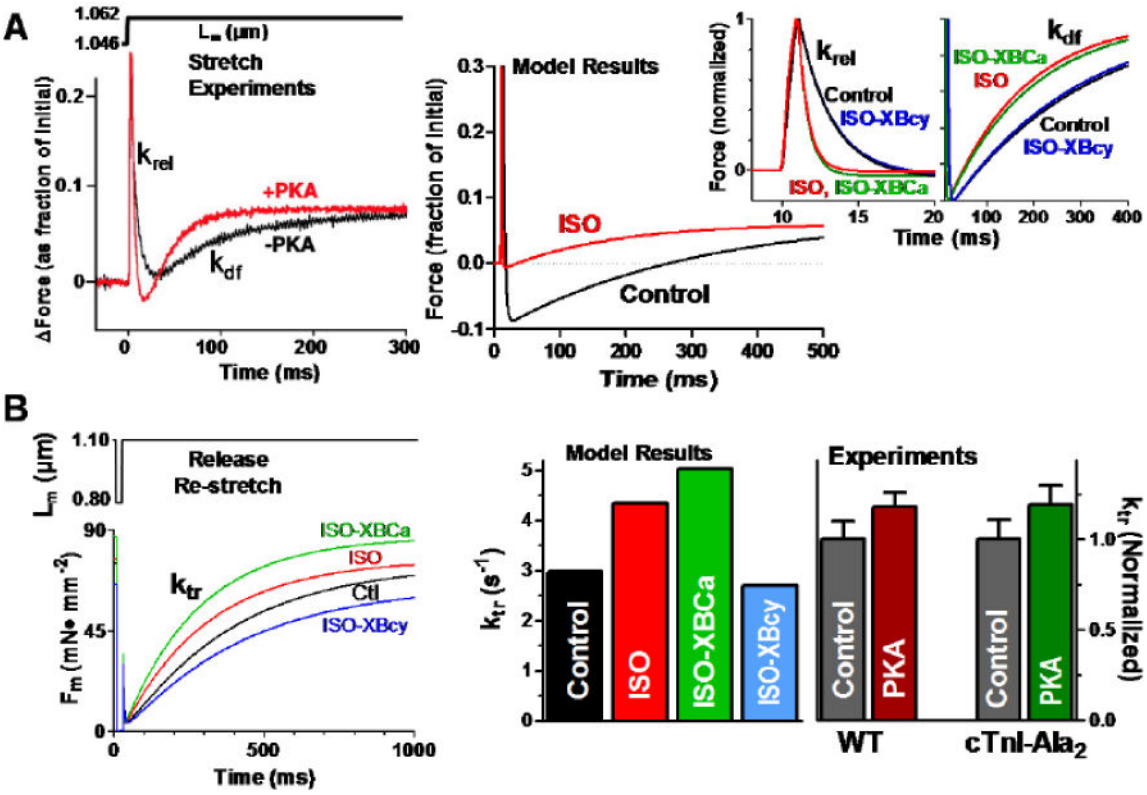

Figure 4.

Contractile response to stretch at fixed $[Ca^{2+}]_i$. **A**: Experimental (left, [21]) and simulated (right) force response to a length step. Simulations at expanded time scale show that the 100 nM [ISO] effect on k_{rel} is comparable to the experimental response in WT mice [21]. ISO-XBCa and ISO-XBcy simulations (insets) evidence a comparable response with non-phosphorylatable TnI (cTnI-Ala2, [21]) and non-phosphorylatable MyBPC (cMyoBP-C(t3SA), [20]) (experimental data not shown). **B**: Simulated force response following a release and restretch pulse (left panel), and simulated and experimental rates of force redevelopment (k_{tr}, right panel). k_{tr} increases in ISO and ISO-XBCa, equivalent to the behavior observed in WT and cTnI-Ala2 mice [23], and decreases in ISO-XBcy (see Table 3 for simulation numerical values).

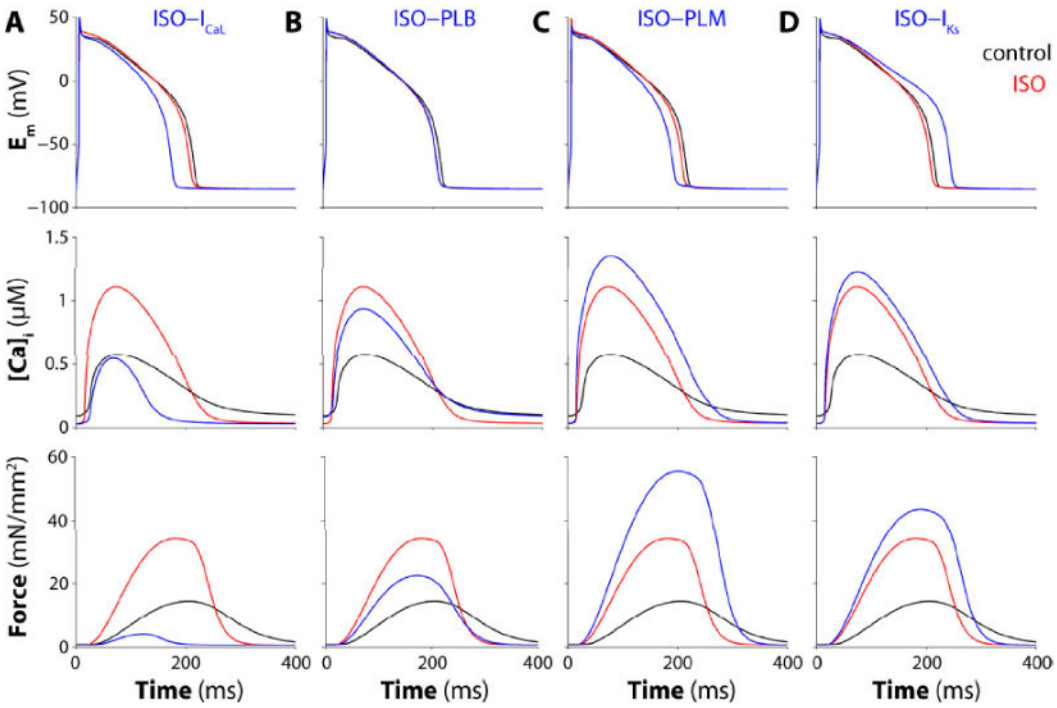

Figure 5.

Effects of PKA-phosphorylation on individual ion channel and transporter targets. Time courses of membrane potential (top panels), Ca^{2+} transient (middle) and isometric force (bottom) during steady state 1-Hz stimulation are shown before (black), with 100 nM [ISO] (red) an with ISO, but with PKA effects on the indicated transporter disabled, for I_{CaL} (**A**), PLB (**B**), PLM (**C**), and I_{Ks} (**D**).

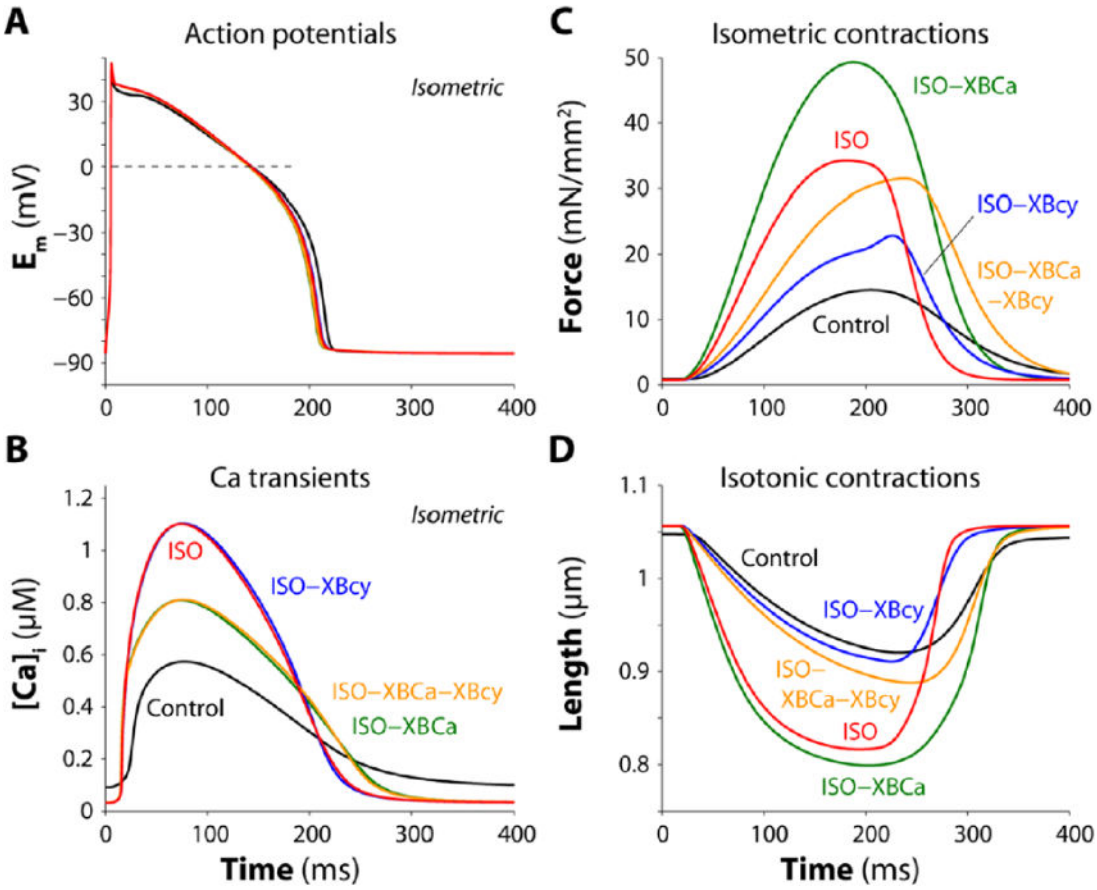

Figure 6.

Simulation of AP, $[Ca^{2+}]_i$ and isometric or isotonic twitches. Results are shown for control, ISO (100 nM), and ISO with suppression of different target effects (ISO-XBCa, ISO-XBcy and ISO-XBCa-XBcy). **A:** ISO slightly reduces APD, a response seen in all β-AS conditions. **B:** ISO and ISO-XBcy increase peak $[Ca^{2+}]_i$, its velocity of rise and faster decline (TCa_{50} and TCa_{90}), while abrogation of conditions involving XBCa decrease the peak $[Ca^{2+}]_i$. **C–D:** ISO increases isometric force and isotonic shortening which is further enhanced upon eliminating ISO effect from XBCa (ISO-XBCa). Abrogation of ISO effect on XBcy (ISO-XBcy) blunts inotropy for force and shortening, while removing ISO effect on both contractile targets (ISO-XBCa-XBcy) allows the inotropic increase in force but not shortening (see also Table 4).

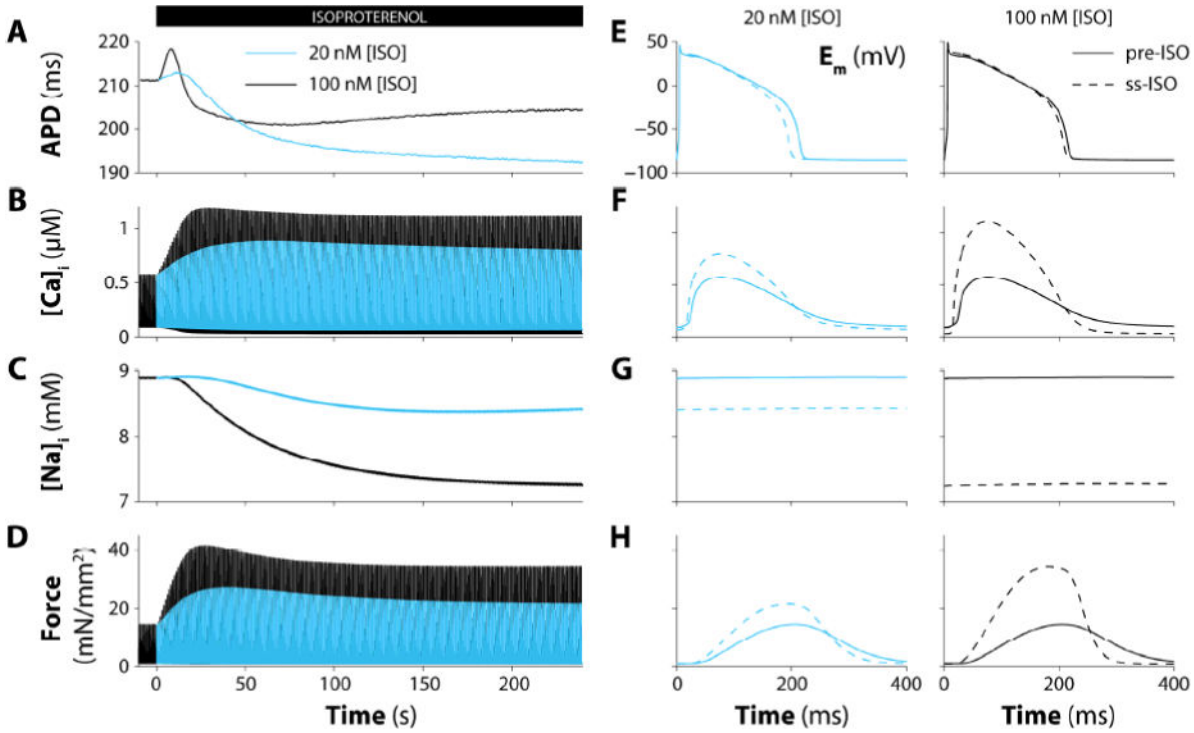

Figure 7.

Time-course and graded effect of β-AS. Simulated action potential duration (**A**), $[Ca^{2+}]i$ (**B**), $[Na^{+}]i$ (**C**), and isometric force (**D**) in virtual myocyte paced at 1 Hz during 4 min exposure to ISO (20 and 100 nM; black and blue). Expanded time scales for membrane potential (**E**), $[Ca^{2+}]i$ (**F**), $[Na^{+}]i$ (**G**), and isometric force (**H**) before (solid) and after (dashed) 20 nM (left) and 100 nM (right) [ISO] administration.

Table 1

Mechanical parameter classification and values.

Role	Symbol	Defining Eq.	Units	Value	Effect of 100 nM [ISO]
Strct	A_p	9, 14, 15	mN mm^{-2} μm^{-1} μM^{-1}	2700	
Strct	A_w	9, 14, 15	mN mm^{-2} μm^{-1} μM^{-1}	540	
Strct	α	13	mN mm^{-2}	0.5	
Strct	β	13	μm^{-1}	80	
Strct	K_e	12	mN mm^{-2} μm^{-5}	105000	50% decrease [56]
Strct	L_e	12	mN mm^{-2} μm^{-1}	10	
Strct	L_o	12	μm	0.97	
Strct	[TSt]	20	μM	23	
XBCa	Y_b	16	μM^{-3} ms^{-1}	0.1816	
XBCa	Y_r	18, 19	ms^{-1}	0.1397	2.2-fold increase [18–22, 63]
XBCa	Z_b	16	ms^{-1}	0.1397	4.2-fold increase [18–22, 63]
XBCa	Z_r	18, 19	μM^{-3} ms^{-1}	7.2626	80% increase [18–22, 63]
XBcy	B_w	10	ms^{-1}	0.35	3.4-fold increase [18–22, 63]
XBcy	B_p	11	ms^{-1}	0.5	3.4-fold increase [18–22, 63]
XBcy	h_{pr}	11	μm	0.006	
XBcy	h_{wr}	10, 23	μm	0.0001	
XBcy	F_h	23	adimensional	0.1 or 1	
XBcy	γ	23	μm^{-2}	28000	
XBcy	L_a	21	μm	1.15	
XBcy	L_c	24	μm	1.05	
XBcy	R_a	21	μm^{-2}	20	40% decrease (model fit)
XBcy	Y_a	21	ms^{-1}	0.0023	24% increase [18–22, 63]
XBcy	Y_c	24	μm^{-1}	4	40% decrease (model fit)
XBcy	Y_d	24	ms^{-1}	0.028	2.2-fold increase (model fit)
XBcy	Y_p	17, 18	ms^{-1}	0.1397	2.2-fold increase [18–22, 63]

Role	Symbol	Defining Eq.	Units	Value	Effect of 100 nM [ISO]
XBcy	Y_v	23	ms^{-1}	0.9	60% increase (model fit)
XBcy	Z_a	22	ms^{-1}	0.0023	24% increase [18–22, 63]
XBcy	Z_p	17, 18	ms^{-1}	0.2095	2.2-fold increase [18–22, 63]

Table 2

Effect of β-AS on ionic model parameters.

Target	Effect of β-AS	Effect of 100 nM [ISO]
I_{CaL}	Enhanced channel opening probability and increased fraction of available channels	8% of channels in gating mode 2 and 29% increase in channel availability
RyR	Enhanced channel opening probability	53% increase in k_{oSRCa}
PLB	Enhanced Ca^{2+}-sensitivity of SERCA	68% reduction of forward mode K_{mf}
PLM	Enhanced NKA activity due to increased affinity for $[Na^+]_i$	K_{mNaip} reduced from 11 to 8 mM
I_{Ks}	Enhanced channel availability and left-shifted current-voltage relationship	2.8-fold increase in channel availability and 15-mV shift
IKr	Enhanced channel availability and left-shifted current-voltage relationship	30% increase in channel availability and 10-mV shift
I_{CFTR}	Graded current activation	Total conductance g_{CFTR} increased to 0.0043 A/F
$I_{Cl(Ca)}$	Increased Ca^{2+}-affinity of the channel	30% reduction in K_{dClCa}

Table 3

Contractile response at imposed $[Ca^{2+}]_i$ in control, ISO, ISO-XBCa, ISO-XBcy, ISO-XBCa-XBcy, and ISO-titin.

Index	Units	Control	ISO	ISO-XBCa	ISO-XBcy	ISO-XBCa-XBcy	ISO-titin
nH	adimensional	4.03	4.00	4.22	3.74	4.03	4.00
$[Ca^{2+}]_{50}$	μM	0.765	1.154	0.801	1.141	0.765	1.154
F_b(max)	mN mm^{-2}	92.5	97.2	97.2	92.5	92.5	97.2
k_{rel}	s^{-1}	39.6	101.9	100.4	40.3	39.8	101.9
k_{df}	s^{-1}	4.15	9.3	8.09	4.48	4.15	9.31
k_{tr}	s^{-1}	2.98	4.34	5.02	2.69	2.98	4.34
Stiff.min	mN mm^{-2} μm^{-1}	70.6	22.2	37.6	36.9	70.6	22.2
Fr(Stiff.min)	Hz	0.85	1.20	1.12	0.85	0.85	1.20
V_{max}	μs^{-1}	1.01	1.62	1.67	0.93	1.01	1.53

The F_b-$[Ca^{2+}]_i$ relationship is characterized by nH, $[Ca^{2+}]_{50}$ and F_b(max) of the Hill equation. k_{rel} and k_{df} describe the response to a length step, and k_{tr} depicts the reaction to a length pulse. Minimum stiffness (Stiff.min) and frequency (Fr) at minimum stiffness (Fr(Stiff.min)) describe the stiffness-frequency relationship, and V_{max} characterizes the response of the force-velocity relationship.

Table 4

Isometric and isotonic twitch responses to ISO, ISO-XBCa, ISO-XBcy, ISO-XBCa-XBcy, ISO-titin, and ISO-Cytofl.

Feature	Units	Control	ISO	ISO-XBCa	ISO-XBcy	ISO-XBCa-XBcy	ISO-titin	ISO-Cytofl
Isometric contractions (L_m = 1.05 μm)								
APD_{90}	Ms	211.3	204.3	201.2	204.9	201.9	204.2	212.1
$[Ca^{2+}]_{CL}$(max)	μM	77.0	228.4	277.7	223.5	272.1	228.4	69.7
$[Ca^{2+}]_{SL}$(max)	μM	5.94	10.00	11.60	9.84	11.41	10.00	5.61
$[Ca^{2+}]$i(max)	μM	0.577	1.110	0.814	1.111	0.816	1.110	0.780
$[Ca^{2+}]_i$(min)	μM	0.091	0.031	0.033	0.031	0.032	0.031	0.090
TCa(max)	Ms	77.3	75.4	73.5	75.3	76.6	74.0	75.2
TCa_{50}	Ms	114.6	105.6	125.7	109.0	125.6	107.3	88.0
TCa_{90}	Ms	213.2	157.2	192.7	154.0	186.5	159.4	167.6
F_m(max)	mN mm^{-2}	14.5	34.3	49.3	22.9	31.5	34.3	12.8
F_m(min)	mN mm^{-2}	0.91	0.76	0.77	0.76	0.77	0.83	0.78
TP_{50}	Ms	107.3	87.4	89.5	109.3	110.6	88.0	85.2
RT_{50}	Ms	93.4	66.2	82.2	46.7	65.4	65.8	68.5
T_{90}	Ms	378.5	280.7	314.2	325.1 87	363.1	279.8	275.4
Isotonic contraction (F_m = 0.87 mN mm^{-2})								
APD_{90}	Ms	211.9	205.5	202.2	206.0	202.2	205.4	212.7
$[Ca^{2+}]_i$(max)	μM	0.580	1.109	0.813	1.106	0.810	1.110	0.787
$[Ca^{2+}]_i$(min)	μM	0.091	0.031	0.032	0.031	0.032	0.031	0.090
TCa(max)	Ms	79.6	77.5	77.3	77.9	77.8	77.2	76.3
TCa_{50}	Ms	115.8	108.6	128.0	109.6	129.4	108.7	90.0
TCa_{90}	Ms	203.6	148.9	182.8	146.7	181.7	149.8	162.2
% short	%	12.1	22.7	24.3	13.8	15.9	21.0	18.3
RT_{50}	Ms	73.9	73.2	105.3	49.5	63.8	78.6	70.6

APD_{90}, APD at 90% repolarization; $[Ca^{2+}]_{CL}$(max) and $[Ca^{2+}]_{SL}$(max), peak in cleft and sub-sarcolemmal $[Ca^{2+}]$; $[Ca^{2+}]_i$(max) and $[Ca^{2+}]_i$(min), peak and minimum in bulk cytosolic $[Ca^{2+}]$; TCa(max), time to $[Ca^{2+}]_i$(max); TCa_{50} and TCa_{90}, time to 50% and 90% $[Ca^{2+}]_i$ decay; TP_{50}, time from the stimulus to 50% peak force; RT_{50}, time from peak force or peak shortening to 50%

relaxation; T_{90}, time from the stimulus to 90% muscle force (F_m) relaxation; $F_m(max)$ and $F_m(min)$, maximum and minimum F_m; % short, percent shortening expressed as the percentage of the difference between maximum and minimum muscle length divided by maximum muscle length.